Universität Stuttgart

Auslandsorientierter Studiengang
Wasserwirtschaft
Master of Science Program
Water Resources Engineering and
Management - WAREM

Master's Thesis:

Numerical Investigations of Flow through Fractured Porous Media

submitted by :

Alexandru-Bogdan Tatomir

Date : **November 29, 2007**

Supervisor : **Prof. Dr.-Ing. Rainer Helmig**
Dr.-Ing. Holger Class

Institut für Wasserbau
Lehrstuhl für Hydromechanik und Hydrosystemmodellierung
Prof. Dr. –Ing. Rainer Helmig
Pfaffenwaldring 61
70569 Stuttgart

CONTENTS

1 INTRODUCTION

The understanding of the multi-phase flow and transport processes in the environmental problems is of capital importance since groundwater is the main source of drinking water supply, agriculture and industry in many places of the world.

The fractured porous media is composed of an interconnected network of fractures and blocks of porous medium. The practical applications are important as many natural formations are fractured, and accurate models are required for predicting the fate of pollutants in aquifers contaminated by industrial, agricultural and radioactive waste.

Fractures occur in different length scale and have a strong influence because most of the flow is concentrated along them. Nevertheless, the rock matrix plays a major role in retarding the migration of the contaminants. It can be asserted that transport in fractured systems is characterized by advection dominating in the fracture and diffusion in the matrix.

Numerical simulation of single and multi-phase fluid flow in fractured media is a challenge for the engineers and researchers. In the study of contaminant transport in fractured porous media, the bulk of the research effort has been devoted to the transport in discrete fracture network models.

Structure of this work

This study starts with an overview of the different fracture-matrix models, describing their strong and weak points, in Chapter 2.

Further on, Chapter 3 discusses the various mathematical models of subsurface flow and the underlying concepts.

Chapter 4 presents an overview of the different numerical methods and then concentrates on the discretization of the two-phase flow equations. For the discrete fracture model approach, a vertex centered finite volume scheme has been chosen due to its monotone behavior and applicability to unstructured multi-element type meshes in two and three space dimensions. The most suitable time discretization is the fully implicit one. For the computation of the single- and two-phase flow equations it was used the modeling system MUFTE-UG. Additionally, Chapter 4 describes the numerical framework UG and the main components that are required by the numerical simulator. Comprehensive numerical results for three different realistic problems involving single- and multi-phase flow in fractured media are then presented in Chapter 5. Finally, the conclusions for the numerical results are drawn in Chapter 6.

Objectives of this work

The first goal of this work is to make a review and compare the different mathematical and numerical models that govern the single and the multi-phase flow systems. In that case, by running the numerical applications which use these theoretical notions we get a quantitative and a qualitative feeling of the processes.

The second goal is to test the capability of the MUFTE-UG flow simulator with regard to the implementation of the lower-dimensional model concept both in two- and three-dimensional domains for one- and two-phase flow problem. Moreover, the capability is tested by comparing the results to the ones given by other flow simulators.

One important aspect that has to be kept in mind is the implementation of the interface conditions into the discretization.

For this it was developed a set of three numerical experiments. All simulations were performed, as it was already mentioned, with MUFTE-UG flow simulator.

The first numerical example belongs to a wider international hydrologic code intercomparison project (HYDROCOIN 1988) where is simulated the steady state flow in a fractured bedrock. The test case is used to verify the capability of MUFTE-UG and to asses the performance of the different representation of the zones.

The second example tests the capability of MUFTE-UG to model two phase flow in 2D fractured porous media using the HYDROCOIN geometry as in the one-phase problem. For the first two numerical simulations the geometries were created using ART (Almost Regular Triangulation) mesh generator.

The third and the final example demonstrates the applicability and the computational advantages of the lower-dimensional fracture approach in three dimensional domain for multi-phase flow. Again, the example was previously investigated in several research works (Zielke et al. [1991], Barlag et al. [1998]). For generating the geometry ANSYS ICEM v.11.0. was used with STAR-CD 3.2.0 solver.

2 FRACTURE MODELS

This chapter introduces the basic considerations for the fracture models and describes the main properties and assumptions for each model.

The topology of the fracture-aquifer systems is difficult to understand due to the fact that fractures occur on a variety of length scales (Figure 1).

One reasonable model for describing fractures is the fractal model since the fractures can be found on the whole range of scales, as shown by *Bonnet et al*. [2001]. A fractal is a "set without a characteristic length scale.

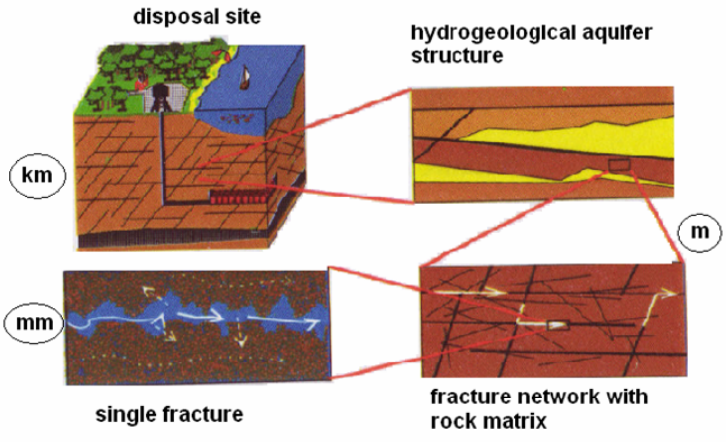

Figure 1: Fractures occurring on different scales (Silberhorn-Hemminger (2002))

Definition

A fracture is generated in a process of cracking where the coherence (cohesion) in the rock is annihilated. A fracture consists of two complementary faces created by the cracking process, the fracture surfaces, with an opening in between.

Principle fracture models

There are three principal fracture models: ***discrete***, ***multi-continua*** and ***hybrid*** models. Figure 2 presents a model with fractures on different scales and the different cut-outs can be described by the different models. (i.e. *cut-out A* is the undisturbed rock matrix and can be described as porous media; *cut-out B*: the highly fissured rock matrix can be considered as a continuum model with an equivalent flow and transport properties; *cut-out C*: the large fractures can be modeled with a discrete model; *cut-out D*: a hybrid models can be applied).

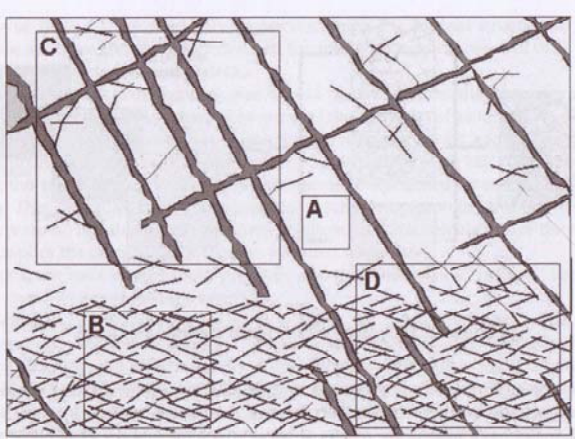

Figure 2: Fractured groundwater aquifer with different discontinuities (Kröhn (1991))

In the following sections, the three fracture-matrix models will be described in more detail. Different conceptual models have been proposed in the literature for flow and transport in fractured media, i.e. *Juanes et al.* [2002].

2.1 Discrete Models

In the study of transport in fractured porous media, the bulk of the research effort has been devoted to the transport in discrete fracture network models. These studies have proven to be useful for understanding transport phenomena and discrete models are required when the continuum approach to the description of the transport problem is not applicable.

In the discrete models fractures are considered as discrete structures. With such a model, we have the possibility to model flow and transport processes very similarly to nature (*Reichenberger et al.* [2004]). Some of the literature for the discrete fracture model has been reviewed in *Sahimi* [1995] and *Bear et al.* [1993].

As the fracture aperture is very small compared to the extension of the rock blocks and as the flow velocities in the fractures are much higher than in the rock matrix due to the higher permeability, the modeling of flow in fractured porous media is very difficult.

Fractures can be modeled as equidimensional elements (which implies very high demands on net generation and the numerical tools for solving the resulting equation system); or lower dimensional elements (also referred in literature as mixed dimensional elements). The modeling of flow perpendicular to the fracture orientation is more difficult to compute, thus strong assumptions are usually required.

The discrete fracture model is numerically superior to the single-porosity model and overcomes limitations of the dual-porosity models (*Hoteit.and Firoozabadi* [2005]) especially because of the

lack of an exchange term between fractures and rock matrix which can be considered an important conceptual advantage (see *Reichenberger et. al* [2006]).However, the applicability of discrete models remains quite limited to field problems as they require the determination of the precise characteristics of the fracture network in its complete detail. Thus in many practical field problems it is worth using continuum models when the conditions necessary to adopt this approach are met.
The solution for this is to use the geostatistical generated data together with the deterministic data for modeling.

2.2 Multi-continua Models

In the multi-continua models the assumption that has to be made is that the representative elementary volume (REV) cannot be obtained only for the porous medium – the rock matrix – but also for the fractured system. Averaged parameters for rock matrix and fracture system are used in multi-continua models.
The transport problem is transformed from the microscopic level to a macroscopic scale at which the problem is expressed in terms of averages of the microscopic quantities. The need to know the exact local characteristics of the whole domain is circumvented by the use of these average quantities.
The size of this REV must be larger than the heterogeneity size and much smaller than the macroscopic length-scale. It follows that the continuum approach is applicable to a fractured porous medium provided that an REV can be determine (*Royer et al.* [2002]).
The continuum approaches approaches can be categorized as follows:

1) phenomenological approaches with which the form of the macroscopic model is postulated on the basis of physical considerations and experimental results;

2) upscaling methods with which the macroscopic model is rigorously derived by starting with the physical behavior at the REV's scale.

Two kinds of continuous models are usually used: *double-continuum models* and *single-continuum models*. In the double continuum-models, the fractured porous medium is represented as two distinct and interacting continua, one consisting of the network of fractures and the other of the porous blocks. The interaction between both continua is formulated by an exchange function as was originally proposed by *Barenblatt and Zheltov* [1960].

In *Bibby* [1981] and *Huyakorn* [1983], *double-continuum* models have been employed for transport of contaminants. In the *singe-continuum* approach, the whole fractured porous domain is represented as an equivalent porous medium.

Royer et al. [2002] presented a method of homogenization for upscaling by multiple scales expansions and obtained different macroscopic single-continuum transport models. The main condition for homogenization is to have a high density of heterogeneities.

The disadvantage of the *dual-porosity* models in view of their strength and simplicity is that they can be mainly used for sugar-cube representations of fractured media (*Karimi-Fard* [2001]). Another limitation is that the method cannot be applied to disconnected fractured media and cannot represent the heterogeneity of such a system. Another shortcoming is the complexity in the evaluation of the transfer function between the matrix and the fractures.

The *single-porosity* model provides the accuracy, but it is not practical due to very large number of grids. A large number of grids is required because of the two different length scales (matrix size and fracture thickness). When the ratio of the two length scales in a fractured system, as well as the permeability ratio of matrix and fracture are very high, the single-porosity approach becomes very inefficient numerically. Whereas the discrete fracture approach does not suffer from this limitation.

2.3 Hybrid Models

Hybrid models represent a combination of the two model types explained (discrete and multi-continua). The fractures on the observation scale are considered discretely and the fractures on the lower scales, with the help of continua models. Assuming fractal properties of the fracture system with respect to all relevant scales, the hybrid model is the only one which is appropriate.

Unfortunately, combining the two models also combines uncertainties. In addition to the difficulties in representing the discontinuities on the observation scale there are now the uncertainties of the model using multi-continua approach. *Wu and Pruess* [2000] have used this approach to model radio nuclide transport in partially saturated fractured rock.

3 MATHEMATICAL MODEL FORMULATION

This chapter presents the most commonly used mathematical model formulations that govern the complex flow behavior for one and multi-phase flow fracture systems. Only, the case of the discrete fracture models is considered.

3.1 Single Phase Flow in Fractured Porous Media

This section describes the existing theories and laws valid for the single phase fluid flow in fractured porous media. We deal with two approaches: the first one considers fractures as filled porous systems and they can be treated using the *Darcy's* law; the second one considers fractures to be open. For the second case *Stokes*, *Reynolds* or the *local cubic law* could be applied.

3.1.1 Darcy's Law

The *generalized Darcy Law* describes the movement of fluid phase in the porous media and states that the velocity vector v is related to the gradient of the pressure p .

$$v = -\frac{K}{\mu}\left(\nabla p - \rho g\right) \qquad (2.1)$$

Here, μ represents the dynamic viscosity, p the pressure, and the K the absolute permeability. The variable $g = [0,0,-g]^T = -g\nabla z$ is the vector of gravity with the z-coordinate pointing in the upward direction.

There are a series of assumptions to be considered, as they are detailed in *Bear* [1972] and *Hornung* [1997], i.e. the flow is laminar and the fluid is assumed to be Newtonian, and that a non-slip boundary condition is valid at the microscopic scale at fluid-solid interfaced.

3.1.2 Single Phase Flow Equations in a Fracture

Many expressions exist for the fluid flow in open fractures. These expressions are usually derived from the Navier- Stokes equations by making certain assumptions and simplifications. Three of them will be presented in the following.

3.1.2.1 Navier Stokes Equation

The most general description of fluid flow in a single fracture is given by the Navier-Stokes (NS) equations which express momentum and mass conservation over the fracture void space (*Brush and Thomson* [2003]).

Considering the steady laminar flow of a Newtonian fluid with constant density and viscosity through a fracture with impervious walls, the NS equations may be written in vector form as [*Bird et al.*, 1960]:

$$\rho\left(u\cdot\nabla\right)u=\mu\nabla^2u-\nabla p \quad , \tag{3.1}$$

$$\nabla\cdot u=0 \quad , \tag{3.2}$$

where ρ is the fluid density, μ is the fluid viscosity, u = (u_x, u_y, u_z) is the velocity vector, and $p(x,y,z)$ is the hydrodynamic pressure. The hydrodynamic pressure at a point in the fracture is simply the difference between the total and static components of pressure which can be given as:

$$p=p_T-\gamma d=\gamma h \quad . \tag{3.3}$$

$p_T(x,y,z)$ is the total pressure, γ is the fluid specific weight, $d(x,y,z)$ is the depth below the free surface, and $h(x,y,z)$ is defined as the hydraulic head.

Equation (3.1) is the momentum or force conservation equation, and equation (3.2) is the mass conservation equation.

The Navier Stokes equations form a nonlinear system of partial differential equations that are difficult to solve in irregular geometries and even in domains with simple geometry, such as a set of parallel plates.

It is a common practice to simplify the NS equations and there are three successive levels of simplification (*Brush and Thomson* [2003])

3.1.2.2 Stokes Equation

The first level of simplification is to assume that the inertial forces in the flow field are negligibly small compared with the viscous and pressure forces. Equation (3.1) reduces to:

$$0=\mu\nabla^2u-\nabla p \ , \tag{3.4}$$

which along with equation (3.2) forms a linear system of equations called the ***Stokes*** or ***creeping flow equations***. This linear system of equations is easier to solve than the nonlinear NS equations; however, the inertial forces must be verified as being negligible. A common measure of the relative

strength of inertial forces to viscous forces in flowing fluids is the Reynolds number. The Reynolds number for flow through a single fracture may be defined as

$$\mathrm{Re} = \frac{\rho l_v U_i}{\mu} = \frac{\rho \langle b \rangle Q}{\mu \langle b \rangle W} = \frac{\rho Q}{\mu W} \quad , \tag{3.5}$$

where l_v is the characteristic length of the viscous forces and U_i is the characteristic velocity for the inertial forces. l_v is defined as mean fracture aperture $\langle b \rangle$ and U_i is defined as the bulk flow rate through the fracture Q. Experimental observations of flow through smooth parallel plates have shown that the critical Reynolds number marking the beginning of turbulence and the dominance of inertial forces in the flow field is approximately 1200 (*Lomize*, [1951]; *Romm* [1966]; *Louis*, [1969]). Considering typical values of subsurface hydraulic gradients, the value of *Re* in natural fractures will be much lower than this critical value; however, experimental observations using natural fracture samples have demonstrated that inertial forces may be non dominant but significant at *Re* values above 1 – 10. Consequently, there have been several theoretical attempts to quantify the influence of inertial forces in single fractures.

3.1.2.3 Reynolds equation

The second level of simplification is to approximate the three-dimensional flow field given by the Stokes equations with a two-dimensional description. Assuming that the variability in the fracture aperture is gradual, then the velocity normal to the fracture walls will be approximately zero ($u_n \approx 0$) and the viscous forces in the flow field will be dominated by the shear forces acting normal to the fracture wall ($\nabla^2 u \approx \partial^2 u / \partial n^2$). Incorporating these velocity conditions into equation (3.4) and assuming that the fracture walls are approximately normal to the z-axis gives

$$0 = \mu \frac{\partial^2 u}{\partial z^2} - \nabla p \quad , \tag{3.6}$$

where $u=(u_x, u_y, 0)$ is a three dimensional velocity vector with a direction parallel to the x-y plane. Incorporating the no-slip condition (u=0) at the fracture walls, equations (3.6) and (3.4) may be integrated across the local aperture as [see Zimmerman and Bodvarsson, 1996]

$$U = -\frac{b^2 \gamma}{12 \mu} \nabla H \quad , \tag{3.7}$$

$$\nabla \cdot (bU) = 0 \quad , \tag{3.8}$$

where $U=(U_x, U_y)$ is the average in-plane velocity vector, H(x,y) is the average hydraulic head, and b(x,y) is the local aperture parallel to the z-axis.

3.1.2.4 Local Cubic Law (LCL)

By combining equations (3.7) and (3.8) we obtain:

$$\nabla\left[\frac{b^3\gamma}{12\mu}\nabla H\right]=0\ , \tag{3.9}$$

which is commonly known as the ***local cubic law*** (LCL) for fluid flow in a rough-walled fracture, since the magnitude of fluid flow through the subdivided or local fracture voids is proportional to the cube of the local aperture.

Although, the LCL is widely used for simulating fluid flow in rough-walled fracture there are more constraints and assumptions as described in *Brush and Thomson* [April, 2003].

Extensions to the local cubic law which incorporate fracture surface roughness can be found in *Singhal, Gupta* [1999].

3.2 Multi-phase Flow in Fractured Porous Media

3.2.1 Multi-phase Flow Equations

The equations that govern the multi-phase flow will be described in this section.

The flow of a single fluid phase is driven by pressure forces due to pressure differences and gravitational forces only. On the other hand, in two or multi-fluid phase systems, a new force is introduced - the capillary force at the interface between the fluid phases. The capillary force has a significant influence on the fluid behavior.

A good explanation of the processes at the pore scale (microscale) together with the transition to the macro-scale is given in *Helmig* [1997] and *Reichenberger* [2004].

Conservation of mass for multi-phase flow with respect to volume can be formulated as

$$\frac{\partial(S_\alpha \phi \rho_\alpha)}{\partial t} + \nabla \cdot (\rho_\alpha v_\alpha) - \rho_\alpha q_\alpha = 0 \ , \tag{3.10}$$

where ϕ is the porosity, S_α is the saturation of phase α, ρ_α the density, t is the time, v_α is an average microscopic pore velocity vector and q_α represents the source term. The porosity ϕ is defined as the ratio of the volume of the pore space over the total volume of a representative elementary volume (REV). The saturation $S_\alpha = \frac{V_\alpha}{V}$ are defined as the ratio of the pore space of an REV occupied by phase α over the total volume of the pore space within this REV.

As for the one fluid phase flow the velocity vector v_α is related to the gradient of the phase pressure p_α by the generalized Darcy law:

$$v_\alpha = -\frac{k_{r\alpha}}{\mu_\alpha} K(\nabla p - \rho_\alpha g) \ , \tag{3.11}$$

Here, $k_{r\alpha}$ represents the relative permeability, μ_α the dynamic viscosity, p_α the pressure of phase α, and the K the absolute permeability. The variable $g = [0, 0, -g]^T = -g\nabla z$ is the vector of gravity with the z-coordinate pointing in the upward direction.

These equations are valid in the matrix and in the fracture if the flow is laminar in both regions. If the fracture is open, the local cubic law (see section 3.1.2.4) can be employed to define the absolute permeability for the flow of a single incompressible fluid phase. The absolute permeability is then $K=b^2/12$ where b is the distance of the two parallel plates.

The general form of the multi-phase flow equation is obtained by inserting (3.11) into (3.10):

$$\frac{\partial\left(S_\alpha \phi \rho_\alpha\right)}{\partial t} - \nabla \cdot \left(\rho_\alpha \frac{k_{r\alpha}}{\mu_\alpha} K \left(\nabla p - \rho_\alpha g \right) \right) - \rho_\alpha q_\alpha = 0 \,. \tag{3.12}$$

For a two-phase flow model of a wetting fluid phase '*w*' and a non-wetting fluid phase '*n*' in a porous medium the equations are:

$$\frac{\partial\left(S_w \phi \rho_w\right)}{\partial t} - \nabla \cdot \left(\rho_w \frac{k_{rw}}{\mu_w} K \left(\nabla p - \rho_w g \right) \right) - \rho_w q_w = 0 \ , \tag{3.13}$$

$$\frac{\partial\left(S_n \phi \rho_n\right)}{\partial t} - \nabla \cdot \left(\rho_n \frac{k_{rn}}{\mu_n} K \left(\nabla p - \rho_n g \right) \right) - \rho_n q_n = 0 \ . \tag{3.14}$$

The coupling of the saturation and pressure is made by:

$$S_w + S_n = 1 \text{ and } \ p_n - p_w = p_c \ . \tag{3.15}$$

The model has to be complemented by appropriate boundary conditions and initial conditions which have to be chosen consistent with equation (3.15).

In conjunction with equation (3.15), the equations (3.13) and (3.14) form a coupled dynamic system of differential equations which has a strong nonlinear behavior because of the nonlinear dependence of the saturation on the capillary pressures and on the relative permeabilities. This nonlinearity is reinforced by the fact that the constitutive relationships, as well as the flow behavior in porous media, can vary strong (*Helmig* [1997]).

There are different ways to formulate the two phase flow equation. For an introduction to different formulations of the multiphase flow equations see also the books by *Peaceman* [1977], *Chavent* and *Jaffré* [1978], *Aziz* and *Settari* [1979] and *Helmig* [1997] The three more representative ways are the following:

- ***pressure formulation*** having pressures as unknowns (primary variables);
- ***pressure-saturation formulation*** having the pressure of the fluid with the highest affinity and the saturation of the other phase as unknowns;
- ***saturation formulation*** having the phase saturations as unknowns.

Helmig [1997] presents these formulations considering a two-phase system with constant porosity in time under isothermal conditions. He concludes that the pressure formulation for the case of fractures or heterogeneous media is very difficult to use due to the fact that the capillary pressure gradient must be greater than zero. Contrary to the pressure formulation, the formulation of the pressure-saturation formulation has the advantage that it can be applied to systems with subdomains of small capillary pressure gradients because the capillary effects are explicitly

included in the system of equations. Nevertheless, *Bastian* [1999] successfully applied both the pressure and pressure-saturation formulations and concluded that the second gives qualitatively and quantitatively better results on coarser meshes and lead to easier to solve linear and nonlinear systems. As for the saturation formulation, a good description is given also in *Helmig* [1997]. *Ersland et al.* [1998] used the fractional flow formulation, (as it is also called global pressure formulation *Bastian* [1999]) for fluid flow in media with heterogeneities.

For the simulations that will presented later in this work it was used the phase pressure-saturation formulation.

3.2.2 Phase Pressure – Saturation Formulation

In the phase pressure –saturation formulation, or PPS formulation, two out of the four variables p_w , p_n , S_w and S_n in the multi-phase flow equations (3.13) and (3.14) can be chosen as independent variables.

For example to obtain the (p_w, S_n) formulation the following substitutions are made:

$$S_w = 1 - S_n \text{ and } p_n = p_w + p_c\left(1 - S_n\right) . \tag{3.16}$$

The formulation based on p_w assume that the water phase exists everywhere in the domain.

$$\frac{\partial\left(\left(1-S_n\right)\phi\rho_w\right)}{\partial t} - \nabla\cdot\left(\rho_w \frac{k_{rw}}{\mu_w} K\left(\nabla p_w - \rho_w g\right)\right) - \rho_w q_w = 0 , \tag{3.17}$$

$$\frac{\partial\left(S_n\phi\rho_n\right)}{\partial t} - \nabla\cdot\left(\rho_n \frac{k_{rn}}{\mu_n} K\left(\nabla p_w + \nabla p_c\left(S_w\right) - \rho_n g\right)\right) - \rho_n q_n = 0 . \tag{3.18}$$

The equations are considered in (0,T) x Ω. $\Omega \subset \mathbb{R}^d$, (d=2,3) is a domain with polygonal or polyhedral boundary or d = 2 and d =3, respectively. The equations are complemented with initial conditions and boundary conditions of Neumann or Dirichlet type on the boundaries Γ_{an} and Γ_{ad}

$$p_w\left(x,0\right) = p_{w0}\left(x\right),\ S_n\left(x,0\right) = S_{n0}\left(x\right)\ \forall x \in \Omega , \tag{3.19}$$

$$p_w\left(x,t\right) = p_{wd}\left(x,t\right) \text{ on } \Gamma_{wd},\ S_n\left(x,t\right) = S_{nd}\left(x,t\right) \text{ on } \Gamma_{wd} , \tag{3.20}$$

$$\rho_w v_w \cdot n = \phi_w\left(x,t\right) \text{ on } \Gamma_{wd},\ \ \rho_n v_n \cdot n = \phi_n\left(x,t\right) \text{ on } \Gamma_{nn} , \tag{3.21}$$

If both phases are incompressible no initial condition for p_w is required. Γ_{wd}^{p} should have positive measure to determine p_w uniquely.

The following dependencies are assumed:

$$g = \text{constant} , \tag{3.22}$$

$$q_\alpha = q_\alpha(x,t) \quad , \tag{3.23}$$

$$p_c = p_c(x, S_w) \ , \tag{3.24}$$

$$k_{r\alpha} = k_{r\alpha}(x, S_\alpha) \ , \tag{3.25}$$

$$\rho_\alpha = \rho_\alpha(p_\alpha) \quad , \tag{3.26}$$

$$\mu_\alpha = \mu_\alpha(p_\alpha) \quad , \tag{3.27}$$

$$\Phi = \Phi(x) \qquad . \tag{3.28}$$

The influence of fractures on the fluid flow is included through the dependency of the quantities in equation (3.28) on the position.

3.2.3 Constitutive relationships

The secondary variables p_c and $k_{r\alpha}$ are related to the primary variables p_w and S_n through constitutive relationships. Various functionals describing these relations can be found in the literature. The widely used capillary pressure - saturation relationships and relative permeability – saturation relationships are given by *Brooks and Corey* [1964] and *Van Genuchten* [1980].

3.2.3.1 Brooks-Corey Relationships

Even though the primary variable is S_n the constitutive relationships can be formulated in terms of the wetting phase saturation S_w as it is the more common notation. The capillary pressure-saturation relationship is:

$$p_c(S_w) = p_d S_e^{-\frac{1}{\lambda}} \qquad , \tag{3.29}$$

$$S_e = \frac{S_w - S_{wr}}{1 - S_{wr}} \qquad . \tag{3.30}$$

Where S_{wr} is the residual saturation of the wetting phase and S_e the effective saturation. The parameters p_d and λ for a given material are determined in fitting the functional to experimental data. λ is related to the pore size distribution. Materials with small variations in pore size have a large λ value while materials with large variations in pore sizes have small λ values. Usually λ is in the range [0.2; 3].

For a wetting phase saturation of 1, $p_c - S_w$ relationship yields the entry pressure p_d of this material. This entry pressure has to be exceeded to displace the wetting phase from the largest occurring pore.

The relative permeability – saturation relationships given by Brooks and Corey can be formulated as:

$$k_{rw} = S_e^{\frac{2+3\lambda}{\lambda}} , \tag{3.31}$$

$$k_{rn} = \left(1 - S_e\right)^2 \left(1 - S_e^{\frac{2+\lambda}{\lambda}}\right) . \tag{3.32}$$

Across the interface between the wetting and the non-wetting phase a jump discontinuity occurs in the pressure, because the pressure p_n in the non-wetting phase is larger than the pressure p_w in the wetting phase. This jump is the capillary pressure p_c

$$p_c = p_n - p_w \geq 0 . \tag{3.33}$$

3.2.3.2 Van Genuchten Relationships

The Van Genuchten capillary pressure function is formulated as follows:

$$p_c\left(S_w\right) = \frac{1}{\alpha}\left(S_e^{-\frac{1}{m}} - 1\right)^{1/n} , \tag{3.34}$$

where $m = 1 - \frac{1}{n}$ and α is related to the entry pressure.

3.2.4 Interface Conditions at Media Discontinuities

The governing equations for two-phase fluid flow in porous media are only valid if the media properties are subject to slow and smooth variation. At media discontinuities with sharp changes in properties like permeability or porosity it is necessary to introduce interface conditions which model the correct physical behavior.

The approach of *van Duijn et al.* [1995] for the treatment of media discontinuities has been adapted to the case of fractured media.

It is known that the capillary forces are responsible for trapping and pooling at media discontinuities. For this reason the effects of capillary force are very important to capture.

The partial differential equations for two-phase flow are of second order in space. Therefore an interface condition at an inner boundary has to consist of two conditions *Helmig* [1997].

1. ***Continuity of flux***: the flux of both phases across the interface has to be continuous

2. ***Continuity of intensive state variables***: the capillary pressure is continuous at the interface

To derive the second condition we consider two parts of the domain, a fracture Ω^f and the matrix Ω^m. A mobile wetting phase in both matrix and fracture is being assumed, hence p_w is continuous across the fracture matrix interface Γ. The absolute permeabilities in their respective domains are:

$$K(x) = \begin{cases} K^f(x) & if\ x \in \Omega^f \\ K^m(x) & if\ x \in \Omega^m \end{cases} . \qquad (3.35)$$

Accordingly, the porosity ϕ depends on the domain as well as the capillary pressure function $p_c(S_w)$ and the relative permeability functions $k_{r\alpha}$. The capillary pressure functions $p_c(S_w)$ are shaped like in Figure 3. *Niessner et al*. [2005] presented a case applying the interface condition in a one dimensional column.

Two assumptions are essential without taking into consideration the blocking fractures (e.g. fractures filled with clay):

- The absolute permeability in the matrix is smaller than the absolute permeability in the fractures, $K^m(x) < K^f(y)$ for all $x,y \in \Omega$.
- The capillary pressure function values in the matrix are larger than the capillary pressure function value in the fractures for the same saturation (the entry pressure of the rock is larger than the fractures).

For the Brooks-Corey capillary pressure relation results the following interface condition:

$$S_w^m = \begin{cases} 0 & if \quad S_w^f > S_w^* \\ \left(p_c^m\right)^{-1}\left(p_c^f\left(S_w^f\right)\right) & if \quad else \end{cases} . \qquad (3.36)$$

The interface condition is graphically represented in Figure 3 and is called ***extended capillary pressure condition.***

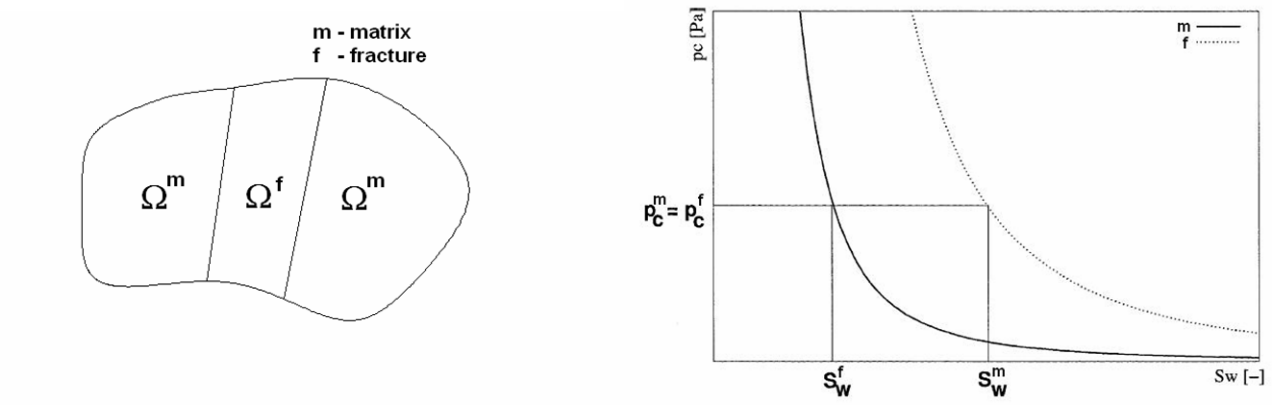

Figure 3: Continuity of the capillary pressure, discontinuity of saturation across the interface. Extended capillary pressure condition

3.2.5 Summary of model assumptions

Contrary to the classical approach to fracture modeling by double porosity models that require different equations for different regions and coupling between the domains is handled by the introduction of exchange terms, the model equations differentiate only in terms of material properties between fractures and matrix.

The first assumption is that the flow regime in both domains is laminar and that an REV can be found for fracture and matrix, therefore, the multi-phase fluid flow equations are valid in the rock matrix and the fractures. The multi-component and non-isothermal behavior of the fluids is not considered.

Another assumption is that the fracture width is orders of magnitude smaller than the fracture length which means that in a 3D domain fractures are of essentially planar geometry. For each point of the fracture the aperture has to be associated.

Going further, it is assumed that the absolute permeability of the fractures is larger than the absolute permeability of the rock matrix. The blocking fractures are not considered, only the open and the filled ones.

Relative permeability functions and capillary pressure functions exist for fractures and matrix. The capillary pressure function is assumed to be strictly monotone decreasing, and it is assumed that the capillary pressure functions for rock and matrix do not intersect.

A last assumption is that the wetting phase exists and is mobile in fractures and rock matrix

4 NUMERICAL MODEL

4.1 Classification of the numerical methods

Hoteit and Firoozabadi [2005] give a good classification of the numerical methods according to spatial approximations. After them the classical finite element methods can be divided into two categories:

1. **vertex based methods**: methods that use nodal or vertex-based representation for the unknowns like Galerkin finite element (FE) and vertex-centered control volume methods
2. **cell-based methods** like cell-centered finite volume (FV), finite differences (FD), discontinuous Galerkin (DG) and mixed finite element (MFE)

According to the spatial approximation of the unknowns each method can be adapted to represent the linear representation of the fractures. Unlike the methods of the first category (*Bastian et al*. [2000], *Karimi-Fard and Firoozabadi*, [2003]; *Monteagudo and Firoozabadi*, [2004]) all methods in the second category face difficulties and therefore need special treatments to handle the hybrid spatial approximations (*Slough et al.* [1999b], *Karimi-Fard et al.*, [2004]; *Granet et al.*, [2001]).
The cell based methods require computing the fluxes across the cell edges.

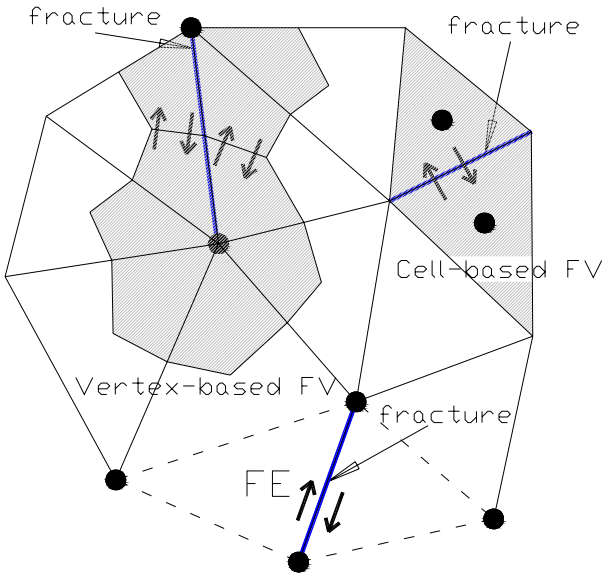

Figure 4: Classification of numerical methods according to spatial approximations

When choosing the numerical model the following considerations have been made:

- The simulator should be applied to problems in fractured porous media from the laboratory scale to the field scale. Thus, the capillary pressure effects have to be captured in accordance to the extended capillary pressure condition of van Duijn.
- The unstructured meshes are absolutely necessary due to the complex geometries we encounter
- The numerical scheme has to be stable, consistent, monotone and mass conservative.
- The stability of the scheme is guarantied for the implicit time discretization, therefore the backward Euler method is going to be employed
- For an efficient implicit scheme a fast solution of the nonlinear systems of equation has to be obtained. Therefore the inexact Newton scheme is being used. The scheme is inexact because it solves the arising linear systems of equations up to a given tolerance. The global convergence of the Newton method is achieved by a line-search algorithm. The linear systems of equations are solved with the multigrid method.

For all these considerations, all the numerical simulations performed with MUFTE-UG used the vertex-centered finite volume method. The method has a monotone behavior, it is locally mass conservative, and can easily be applied to unstructured grids. Thus, it is important to understand the vertex centered finite volume method and it will be described in the following section. A good description of it for the phase-pressure-saturation formulation and with the implementation of the lower-dimensional fracture model concept can be found in *Reichenberger et. al* [2006]. In the same time finite vertex centered finite volume methods are presented in *Helmig* [1997]. Applications of the vertex centered finite volume method are found in *Bastian* [1999], *Gebauer et. al* [2002], *Niessner et al.* [2005], *Reichenberger et al.*[2004] and [2006].

4.2 The Vertex Centered-Finite Volume Method

This section will be presents the spatial discretization schemes for the discrete fracture model concept.

The vertex centered finite element method is found in the engineering literature as *control volume FEM (Reichenberger et al.*[2004]), box method or subdomain collocation finite volume method (*Helmig* [1997]).

For the numerical solution of the multi-phase fluid flow equation one important simplification is made by employing lower dimensional elements or Indshell. The models are then called lower-dimensional models or mixed-dimensional models.

4.2.1 Fracture geometry formulation

The assumptions on the fracture network are essential for the discretization method. In the following, superscript '*m*' denotes entities in the volumetric rock matrix and superscript '*f*' denotes entities in the fracture network.

For beginning, $\Omega \subset \mathbb{R}^d$ is defined as a polygonal (d =2) or polyhedral (d = 3) domain and it contains a non-empty set of fractures $\{f_1 \ldots . f_F\}$. Each fracture f_i is a (d – 1) – dimensional object. Each fracture f_i is identified by its middle surface and has width δ_i associated with it, which may be variable in the fracture. For simplicity the fractures are assumed to have a planar geometry: in two-dimensional domain the fractures are line segments and in a three-dimensional domain they have polygonal shapes.

The *fracture network* is constituted by the union of all fractures $\Omega^f = \bigcup_{i=1}^{F} f_i \subset \Omega$, whereas, the domain of the rock matrix Ω^m is the whole domain $\Omega^m = \Omega$. The domain of the fracture network overlaps with the rock matrix.

4.2.2 Finite volume grids and the dual grids

Primary Mesh – Finite element mesh

The discretization method requires a mesh for Ω^m and Ω^f. For the volumetric mesh a subdivision E_h^m of Ω^m into K^m elements is considered, $E_h^m = \left\{\Omega_1^m, ..., \Omega_K^m\right\}$ with $\bigcup_e \overline{\Omega_e^m} = \overline{\Omega^m}$ and $\Omega_e^m \cap \Omega_{e'}^m = \varnothing$ for $e \neq e'$. Ω_e^m is the open subdomain covered by the element with index e. h denotes the diameter of the largest element. The subdivision has to resolve the geometry of the fractures comparable to domains with inner boundaries.

To get a better understanding how the vertex-centered finite volume method is implemented, a two-dimensional mesh for a fractured domain is given in Figure 5. The volumetric elements Ω_e^m of E_h^m are triangles or quadrilaterals in two dimensions. Hybrid grids (grids of lower-element type)

are admissible, but require that E_h^m is a triangulation, which is that no vertex of an element lies in the interior of a side of another element.

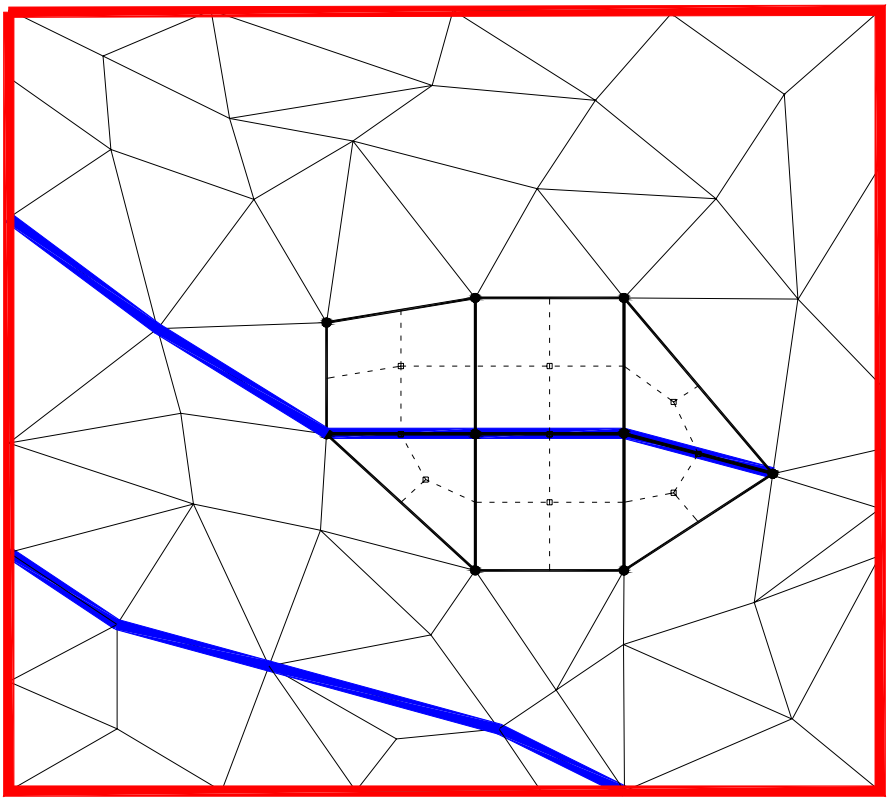

Figure 5: Example domain with fractures and mesh resolving the fracture network geometry

Lower- and equi- dimensional approach

In the lower-dimensional approach, the volumetric elements are complemented with lower dimensional elements on the fractures which are line elements for two-dimensional problems and triangles or quadrilaterals for three-dimensional problems. The fractures appear as inner boundaries to the domain where material properties change. The fracture elements constitute a mesh $E_h^f = \left\{\Omega_1^f, ..., \Omega_{K^f}^f\right\}$ which is conforming with the volumetric mesh; i.e. each Ω_e^f is an element face or face for the two-dimensional and three dimensional case, respectively.

For the equi-dimensional approach both fracture and matrix elements have the same dimensionality, being triangles or quadrilaterals for two-dimensional problem and tetrahedral and prisms for three-dimensional problem (Figure 7).

Secondary mesh – Finite volume mesh

The vertex centered finite volume method requires the construction of a so-called secondary mesh which is done by connecting element barycenters with edge midpoints as shown in Figure 6 in two dimensions. In three dimensions, first the element barycenters are connected to face barycenters and then the grids are denoted by v_i and their corresponding coordinate vector by x_i. By construction each control volume contains exactly one vertex v_i is denoted by b_i^m, thus $B_h^m = \left\{ b_1^m, ..., b_{N^m}^m \right\}$ For two-dimensional fractures, the dual grid is generated in a similar manner. One-dimensional elements are simply divided into parts of equal length. This construction results in a conforming dual mesh for volumetric and fracture elements. The fracture dual mesh is denoted $B_h^f = \left\{ b_1^f, ..., b_{N^f}^f \right\}$.

The fracture and matrix control volumes are related via $b_i^f = b_i^m \cap \Omega^f$ (Figure 6).

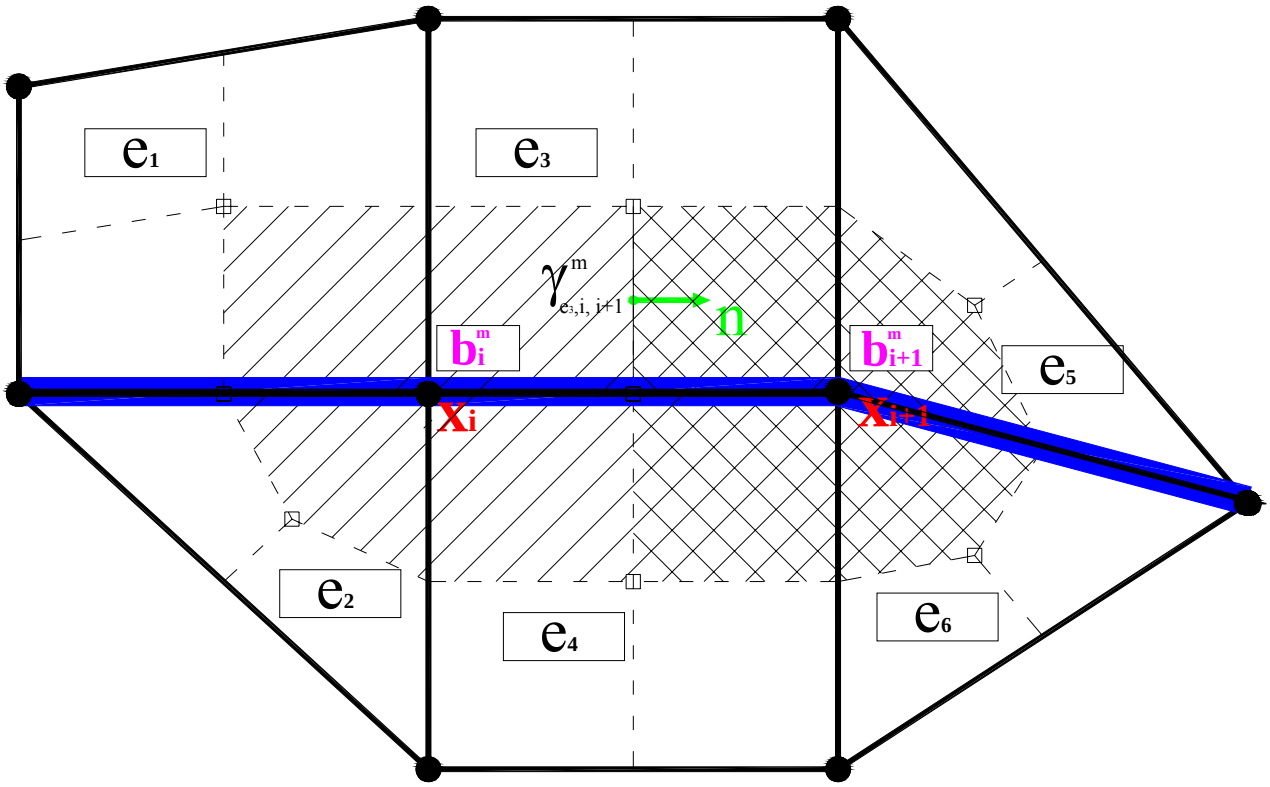

Figure 6: Mesh, dual grid and fracture elements/volumes

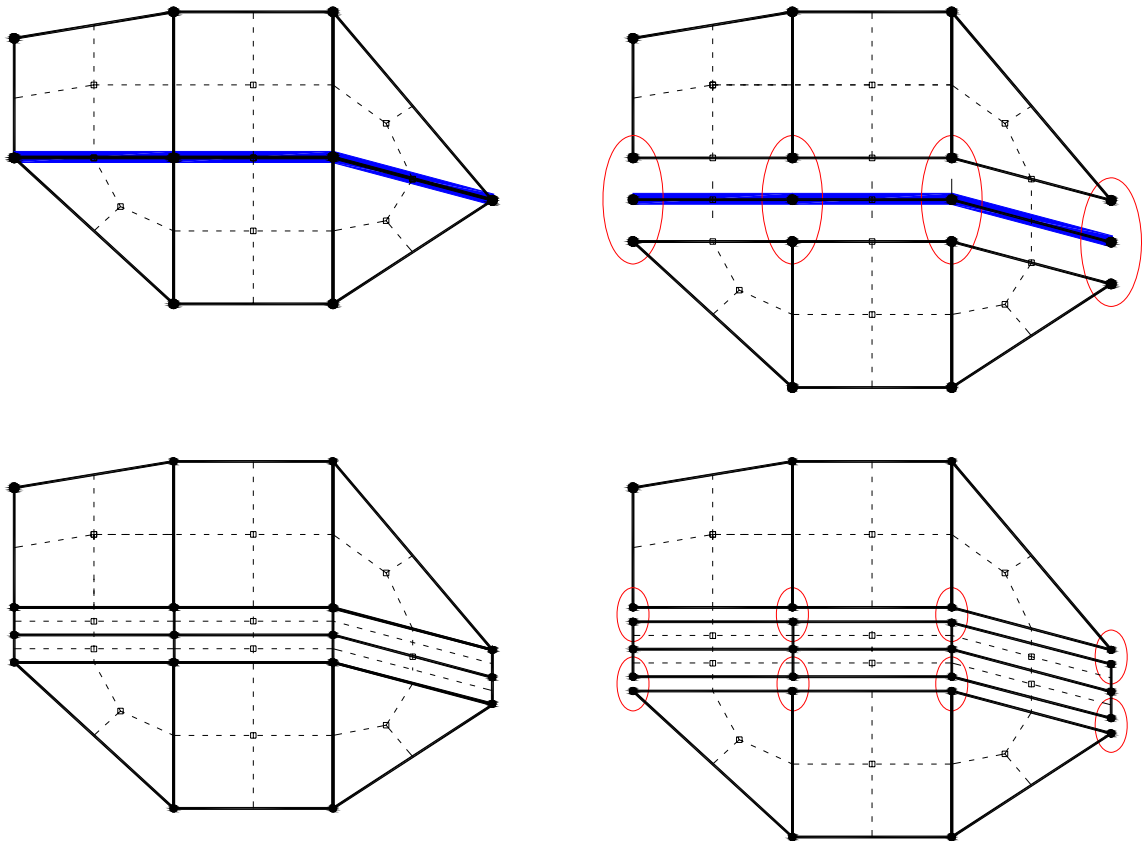

Figure 7: Lower- and equi-dimensional approach for vertex centered finite volume method

With each interface between control volumes a fixed unit normal **n** is associated. The sign of **n** is chosen arbitrarily, but fixed – a possible choice is to let **n** point from the element with the larger index to the element with the lower index.

For any function f defined on Ω^m or Ω^f, which may be discontinuous on the interfaces between rock matrix and fracture the jump of f at point x is defined:

$$[v](x) = \lim_{\varepsilon \to 0+} v(x + \varepsilon n) - \lim_{\varepsilon \to 0+} v(x - \varepsilon n) \ , \tag{4.1}$$

where **n** is the normal to the interface between the control volumes .

For the discretization, the standard conforming, piecewise linear finite element spaces are being introduced in the matrix and fracture domains as in *Reichenberger* [2004] and afterwards the basis functions are defined. In Figure 8 is represented an example for two basis functions.

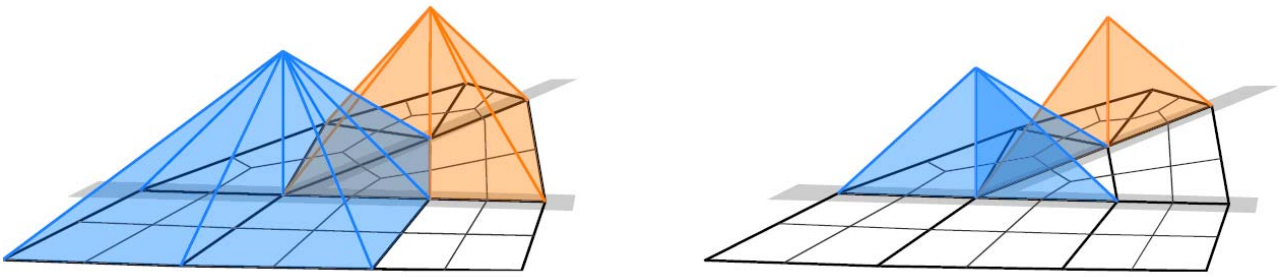

Figure 8: Basis functions for volumetric elements and fracture elements (Reichenberger (2004))

In the case of mixed Dirichlet and Neumann boundary conditions it is necessary to employ separate function spaces for water pressure and non-wetting phase saturation, which adhere to the respective boundary conditions.

The phase saturations S_n and S_w are discontinuous at interfaces between media with different properties as well as at all vertices $v_i \in \Omega^f$, because these vertices are shared by the rock matrix and the fracture network. A discontinuous saturation cannot be represented by the standard conforming finite element spaces so instead the discontinuous saturation spaces have to be chosen.

By means of the mappings, which employ the extended interface conditions it is possible to formulate the discretization by the conforming finite element functions, but to employ the correct discontinuous saturation function wherever appropriate. For more details see *Bastian* [1999], *Reichenberger* [2004].

To implement the transition condition in the vertex-centered finite volume method to each node of the finite element mesh is associated a minimum capillary pressure $p_{c\,min}(x_i)$. If the node is not on the interface then $p_{c\,min}(x_i) = p_c\,(S_{w,i})$ but if it is on the interface then the $p_{c\,min}(x_i)$ is the minimum over all domains having x_i on its boundary.

Assuming that v_h is the finite element function representing non-wetting phase saturation the nodal values S_i^e in element Ω_e^m are found by

$$S_i^e = \begin{cases} v(x_i) & \text{if} \quad p_c\left(x^e, 1 - v(x_i)\right) = p_{c\,\min}(x_i) \\ 0 & \text{if} \quad p_{c\,\min}(x_i) < p_c\left(x^e, 1\right) \\ 1 - S & \text{else, with } S \text{ from } p_c\left(x^e, S\right) = p_{c\,\min}(x_i) \end{cases} . \qquad (4.2)$$

Here the minimal capillary pressure function $p_{c\,\min}(x_i)$ it is employed with nodal values defined as

$$p_{c\min}(x_i) = \min_{\Omega_e \in E(x_i)} p_c\left(x^e, 1 - v(x_i)\right) \tag{4.3}$$

and the barycenters of element *e* are denoted as $\mathbf{x^e}$. $E(x_i)$ is the set of all elements which contain $\mathbf{x_i}$ in their closure.

For fractures the same construction is employed, only that the fracture basis functions are used instead of matrix basis functions.

By defining projections the matrix and fracture finite element spaces can be connected. Let the projection of the test spaces be defined as in *Reichenberger* [2006], $w_h^f(x_i) = w_h^m(x_i)$.

4.2.3 Weak formulation

The weak formulation of equations (3.17)(3.18) for the rock matrix is found by multiplying with the test functions and integration by parts. We employ the following forms in the formulation of the weak form for the rock matrix:

$$m_w^m\left(p_{wh}^m, S_{nh}^m, w_{wh}^m\right) := \sum_{b^m \in B_h^m} \int_{b^m} \phi \rho_w \left(1 - S_{nh}^m\right) w_{wh}^m dx \ , \tag{4.4}(a)$$

$$a_w^m\left(p_{wh}^m, S_{nh}^m, w_{wh}^m\right) := \sum_{\gamma^m \in \Gamma_{\text{int}}^m} \int_{\gamma^m} \rho_w v_w^m \cdot n \left[w_{wh}^m\right] ds$$

$$+ \sum_{\gamma^m \in \Gamma_{ext}^m \cap \Gamma_{wn}} \int_{\gamma^m} \phi_w w_{wh}^m ds$$

$$- \sum_{b^m \in B_h^m} \int_{b^m} \rho_w q_w w_{wh}^m dx \tag{4.4}(b)$$

$$m_n^m\left(p_{wh}^m, S_{nh}^m, w_{nh}^m\right) := \sum_{b^m \in B_h^m} \int_{b^m} \phi \rho_n S_{nh}^m w_{wh}^m dx \ , \tag{4.4}(c)$$

$$a_n^m\left(p_{wh}^m, S_{nh}^m, w_{wh}^m\right) := \sum_{\gamma^m \in \Gamma_{\text{int}}^m} \int_{\gamma^m} \rho_n v_n^m \cdot n \left[w_{nh}^m\right] ds$$

$$+ \sum_{\gamma^m \in \Gamma_{ext}^m \cap \Gamma_{nn}} \int_{\gamma^m} \phi_n w_{nh}^m ds$$

$$- \sum_{b^m \in B_h^m} \int_{b^m} \rho_n q_n w_{nh}^m dx \ . \tag{4.4}(d)$$

where p_{wh}^m belongs to a standard conforming piecewise linear finite element space in the matrix, S_{nh}^m belongs to a discontinuous saturation space and $w_{wh}^m, w_{nh}^m \in W_h^m$ are test functions. γ^m are the interfaces between two control volumes and Γ_{int}^m represents the matrix volumetric dual grid.

The terms in m_α^m are called *accumulation term* and the terms a_α^m are called *internal flux term*, *boundary flux term* and *source and sink term,* respectively. For the numerical evaluation of the accumulation term a midpoint rule is employed, which corresponds to the mass lumping approach in the finite element method.

The Darcy velocities in the interior flux terms are evaluated with an upwind scheme. For the water phase this is for a given control volume face $\gamma_{e,i,i+1}^m$.

$$\int_{\gamma_{e,i,i+1}^m} \rho_w v_w^m \cdot n[w_h]ds = \int_{\gamma_{e,i,i+1}^m} \rho_w \lambda_{w\gamma_{e,i,i+1}^m}^* \tilde{v}_w^m \cdot n[w_h]ds \ , \tag{4.5}$$

with the upwind evaluation of the mobility

$$\lambda_{w\gamma_{e,i,i+1}^m}^* = (1-\beta)\lambda_{wh}\left(x^{\gamma_{e,i,i+1}^m}\right) + \beta \cdot \begin{cases} \lambda_{wh}(x_i) & if\ \tilde{v}_w^m \cdot n \geq 0 \\ \lambda_{wh}(x_{i+1}) & else \end{cases} \ , \tag{4.6}$$

and the directional part of the velocity

$$\tilde{v}_m = -K\left(x^e\right)\left(\nabla p\left(x^{\gamma_{e,i,i+1}^m}\right) - \rho_w\left(x^{\gamma_{e,i,i+1}^m}\right)g\right) \tag{4.7}$$

$x^{\gamma_{e,i,i+1}^m}$ is the barycenter of $\gamma_{e,i,i+1}^m$ and x_i is the grid vertex inside control volume b_i^m. The source and sink terms and the boundary flux terms are evaluated by the midpoint rule. The analogous evaluation scheme is employed for the non-wetting phase saturation. The parameter β controls the upwinding strategy. For β =1 full upwinding is achieved, while β =0 results in a central differencing scheme.

The corresponding forms $m_\alpha^f(\cdot,\cdot,\cdot)$ and $a_\alpha^f(\cdot,\cdot,\cdot)$ for the fractures are derived by replacing superscript 'm' with 'f'

$$m_w^f\left(p_{wh}^f, S_{nh}^f, w_{wh}^f\right) := \sum_{b^f \in B_h^f} \int_{b^f} \phi\rho_w\left(1-S_{nh}^f\right)w_{wh}^f \delta dx \ , \tag{4.8)(a}$$

$$a_w^f\left(p_{wh}^f, S_{nh}^f, w_{wh}^f\right) := \sum_{\gamma^f \in \Gamma_{\text{int}}^f} \int_{\gamma^f} \rho_w v_w^f \cdot n\left[w_{wh}^f\right]\delta ds$$

$$+ \sum_{\gamma^f \in \Gamma_{ext}^f \cap \Gamma_{wn}} \int_{\gamma^f} \phi_w w_{wh}^f \delta ds$$

$$- \sum_{b^f \in B_h^f} \int_{b^f} \rho_w q_w w_{wh}^f \delta dx \ , \tag{4.8) (b}$$

$$m_n^f\left(p_{wh}^f, S_{nh}^f, w_{nh}^f\right) := \sum_{b^f \in B_h^f} \int_{b^f} \phi\rho_n S_{nh}^f w_{wh}^f \delta dx \ , \tag{4.8) (c}$$

$$a_n^f\left(p_{wh}^f, S_{nh}^f, w_{wh}^f\right) := \sum_{\gamma^f \in \Gamma_{\text{int}}^f} \int_{\gamma^f} \rho_n v_n^f \cdot n\left[w_{nh}^f\right] \delta ds$$

$$+ \sum_{\gamma^f \in \Gamma_{ext}^f \cap \Gamma_{nn}} \int_{\gamma^f} \phi_n w_{nh}^f \delta ds$$

$$- \sum_{b^f \in B_h^f} \int_{b^f} \rho_n q_n w_{nh}^f \delta dx \qquad (4.8)\ (d)$$

Here function δ(x) denotes the width of the fracture. In the evaluation of these terms the lower dimensions of the integrals has to be taken into account by using appropriate integral transformations and in the evaluation of the directional velocity.

4.3 Time discretization

The traditional approach to the numerical solution of time-dependent partial differential equations is by the method of lines. First, a spatial discretization is applied to the problem (i.e. the finite volume method) which leads to a system of ordinary differential equations. This system is then solved by a time differencing scheme which can be chosen from the wide range of available methods. The arising system of ordinary differential equations is stiff and should be treated by implicit methods.

The time interval $(0,T)$ is divided into discrete time steps

$$0 = t^0, \ldots, t^M = T$$

of variable or fixed size and the superscript n notation is employed for functions and coefficient vectors denoting values at time step t^n:

$$p_{wh}\left(t^n\right) = p_{wh}^n \text{ and } S_{nh}\left(t^n\right) = S_{nh}^n \ .$$

The standard (multi)-linear nodal finite element basis is employed and this introduces a unique relationship between the discrete functions p_{wh} , S_{nh} and their coefficient vectors $\mathbf{p}_w$ and $\mathbf{S}_n$.

The application of the finite volume discretization scheme leads to the semi-discretization

$$\frac{\partial}{\partial t} M_w\left(p_w(t), S_n(t)\right) + A_w\left(p_w(t), S_n(t)\right) = 0 \ , \qquad (4.9)$$

$$\frac{\partial}{\partial t} M_n\left(p_w(t), S_n(t)\right) + A_n\left(p_w(t), S_n(t)\right) = 0 \ , \qquad (4.10)$$

where $\boldsymbol{M}$ corresponds to m and $\boldsymbol{A}$ corresponds to a. The system can be written as

$$\begin{pmatrix} M_{ww} & M_{wn} \\ M_{nw} & M_{nn} \end{pmatrix} \begin{pmatrix} \dfrac{\partial p_w(t)}{\partial t} \\ \dfrac{\partial S_n(t)}{\partial t} \end{pmatrix} \begin{pmatrix} A_w(p_w, S_n) \\ A_n(p_w, S_n) \end{pmatrix} = 0 \tag{4.11}$$

with submatrices

$$\left(M_{\alpha w}\right)_{ij} = \frac{\partial M_{\alpha w,i}}{\partial p_{w,j}}, \left(M_{\alpha g}\right)_{ij} = \frac{\partial M_{\alpha g,i}}{\partial S_{n,j}} \ . \tag{4.12}$$

This results in a system of differential algebraic equations (DAE) of index 1 in implicit form. The matrix **M,**

$$M = \begin{pmatrix} M_{ww} & M_{wn} \\ M_{nw} & M_{nn} \end{pmatrix}, \tag{4.13}$$

is singular in the incompressible case. An analysis for the incompressible case shows that a discrete form of the elliptic equation has to be satisfied. This is called the implicit constraint. For this reason explicit methods cannot be used for the fully coupled system. One backward Euler step guarantees the validity of the implicit constraint. Time steps computed with other choices than θ =1 in the one step θ method below do not fulfill this property, but they leave the implicit constraint fulfilled if it is satisfied in the preceding time step. For this reason, we always employ one backward Euler step as the first time step, regardless of the time differencing scheme of the subsequent steps.

The time step scheme in the one step θ notation reads as follows.

For n = 0,1, …,M -1 find p_w^n, S_n^n such that for α = w,n

$$M_\alpha^{n+1} + M_\alpha^n + \Delta t^n \theta \left(A_\alpha^{n+1}\right) + \Delta t^n \left(1-\theta\right)\left(A_\alpha^n\right) = 0 \ . \tag{4.14}$$

For θ=1 this yields the backward (or implicit) Euler scheme, θ=1/2 yields the Crank-Nicholson scheme. The implicit Euler scheme is first-order accurate and has very good stability (strongly A-stable)

Equation (4.14) results in a large system of nonlinear algebraic equations. This system is solved using Newton's method and the arising linear systems are solved with a geometric multigrid method.

For MUFTE-UG application

The time discretization used for solving the examples in this work is the implicit finite difference scheme (backward Euler). There is no limit to the time step size considering the stability of the

solution (*Hinkelmann* [2003]). On the other hand, the time step should not be chosen to big considering the accuracy of the solution.

$$\frac{du}{dt} = f(u) \ ,$$

$$\frac{u^{n+1} - u^n}{\Delta t} = f\left(u^{n+1}\right) \ .$$

The implicit time discretization generates large nonlinear systems of equations. The highly nonlinear equation system is handled using the inexact Newton-Raphson algorithm. The linearized systems in the Newton method is solved efficiently by multigrid methods, accelerated by Bi-Conjugate Gradient Stabilized solver (Bi-CGSTAB or referred as *bcgs* in the script file in MUFTE) which is a a Krylov-subspace method.

The performance of the numerical simulator in a vertex-centered finite volume method by using different linearization schemes was investigated in *Niessner et al.* [2005].

4.4 Computer Program MUFTE-UG

The numerical simulator used to compute the results of this work is MUFTE-UG. It can be applied to simulate single and multi-phase flow in fractured porous media and requires several software components which need to interact.

The geometry of domains in the subsurface can be resolved, in all but the simplest cases, only by unstructured grids. The occurrence of sharp front suggests that adaptive grid refinement is employed. A combination of unstructured grids, adaptivity and parallelization introduces complexity into the code development which is by orders of magnitude greater than for structured, uniformly refined grids on a single processor computer. Since it is not reasonable to implement this functionality individually for each application domain, the framework UG was developed, which provides the mentioned functionality in a problem-independent way. The code developed for the solution of the two-phase equations is part of a larger simulation environment, which contains different models for subsurface flow and transport.

In this section will be described some core features of the framework UG and explained how the implementation of the module for fractured porous media is done based on this framework.

4.4.1 MUFTE-UG

The modeling system MUFTE-UG, especially the processing part, is introduced as an example of a numerical simulator in environmental water. MUFTE-UG is a combination of MUFTE and UG. MUFTE stands for Multi-phase Flow, Transport and Energy model, and this software toolbox mainly contains the physical model concepts and discretization methods for isothermal and non-isothermal multi-phase-multicomponent flow and transport processes in porous and fractured-porous media. UG is the abbreviation for Unstructured Grids, and this toolbox provides the data structures and fast solvers for the discretization of partial differential equations based on parallel, adaptive multigrid methods. MUFTE is implemented based on UG.

4.4.2 The Numerical Framework UG

UG was written to provide a framework on which state-of-the-art simulation environments can be built. Many components that are required for the finite element or finite volume simulation of processes described by partial differential equations are independent of the problem, but are so complex that they cannot be implemented by one developer alone. With a framework like UG, developers can focus on modeling, discretization or solvers and don't need to know how load balancing, parallel load migration work in detail.

Domain module:

The domain module can represent two-dimensional and three-dimensional geometries. With the domain manager module domain boundaries can be defined by means of boundary patches and domains can be split into several subdomains (with different material properties). It also handles the treatment of boundary conditions, so that for given nodes or element sides of the grid the user program can determine which boundary condition is valid in a given location. This works also if the grid is distributed over several processors. Inner boundaries are used to describe fractures and to associate a virtual width with each point on the fractures.

Grid manger

UG can handle triangles and quadrilaterals for two-dimensional geometries and tetrahedrons, pyramids, prisms and hexahedrons for three-dimensional geometries. This variety of element types is necessary to maintain consistent grids in adaptive refinement (i.e. no hanging nodes will occur). The different element types also offer flexibility in the triangulation of complicated geometries.

Local grid refinement greatly reduces storage requirements for problems where sharp fronts or singularities in the solution require grid refinement only in certain regions of the domain.

Grids are stored in hierarchical fashion. The hierarchical viewpoint is maintained throughout all components of the UG framework and is used to ensure scalability of all components.

Automatic Grid Generation

Interfaces to different grid generator softwares exist as well as two grid generators which are included with UG, one for two-dimensional domains and one for three-dimensional domains. Additionally there are interfaces to several other grid generators.

User Data Manager

The basic vector matrix data structure is very flexible and allows for the attachment of degrees of freedom with nodes, edges, faces or elements. Based on the user data managers functionality, finite element methods and finite volume method can be implemented from simple node based schemes to complex higher-order methods.

Numerical Algorithms

The numerical algorithms for the solution of linear and non-linear systems as well as the time-stepping schemes are organized in a class hierarchy. The object-oriented approach makes designs of solutions schemes possible which are structurally clear, easily configurable and extensible. The algorithms are implemented in a problem-independent way. Components of a solution scheme can be chosen form a wide range of implemented classes.

Script Language

UG applications are driven by a script language. Its syntax is similar to C. UG applications can either be run in batch mode by executing scripts, or interactively.

Visualization module

The visualization module of UG was designed in a scalable way, so that large parallel simulations can be visualized in an efficient way. It employs the hierarchical data structure and is parallelized, thus avoiding unnecessary calculations in the process. Output can be drawn to the screen or to PostScript or PPM files (as well as to a native picture format)

For more sophisticated visualization it is possible to write data in several visualization program formats: OpenDX/ Data Explorer, TecPlot, GAPE and AVS.

Tecplot[1]

[1] Tecplot is not a part of UG framework but the code in MUFTE is written to generate result files especially to be visualized with Tecplot.

The simulation results are visualized with Tecplot 360. Tecplot 360 is a CFD & Numerical Simulation Visualization Software that allows 2D and 3D visualization.

I/O and restart

In long simulations runs it is often necessary to save intermediate results from which the calculation can be restarted if a hardware error occurs and prevents the simulation from finishing. On parallel computers with several hundreds of processors, this event is much more common than scientists would hope, and on many large computers there is a time limit for individual jobs which is easily exceeded by large simulation runs. In both cases the restart functionality is necessary.

Message Passing Parallelization

UG is parallelized by a domain decomposition approach. An underlying framework, DDD (Dynamic Distributed Data) is responsible for the consistency of the data structures during all stages of the lifetime of an application, especially after modification and distribution of the grid. DDD is also responsible for packing messages, sending them to processors and unpacking them. The passing of messages is done with the functionality of the underlying Parallel Processor Interface (PPIF), which uses MPI, PVM or vendor-dependent message passing mechanisms.

Software Engineering

The large complexity of UG results in a code basis of over 350.000 lines which were written in more than twelve years by seven main developers and numerous other contributors.

All these components work regardless of the underlying physical problem. If solver components are not suitable for the underlying problem it is usually easy to extend the concerning module by inheriting from the solver class and then modifying or extending its functionality.

Knowledge about the physical problem is part of the problem classes. These modules are implemented on top of UG and contain one or several discretizations of the mathematical description of the physical problem along with problem specific functionality like e.g. constitutive relationships.

4.4.3 Mesh Generation

ART (Almost Regular Triangulation)

ART is an automatic grid generator developed by Fuchs [1999] in close collaboration with the research groups in Heidelberg and Stuttgart to meet the special demands required.

The amount of work to create meshes by hand is prohibitive and therefore in the case of complex geometries the multigrid method is inefficient. For this reason it is necessary to use an automatic grid generator.

The lower-dimensional modeling of the fractures is advantageous in the grid generation process because fractures have only to be treated like inner boundaries. This is much easier than the mesh generation for fracture-matrix systems which are represented as thin layers. In the latter case, grid refinement along fractures has to be employed to avoid the creation of excessively many elements in the surrounding rock matrix.

A specific format of the domain is required for ART. First are declares the total number of vertices, edges, faces and elements. For a 2D domain the "Element Number" is zero.

Afterwards are defined:

- the coordinates of the vertices
- the edge numbers
- the face numbers

The number of vertices, edges, faces can be divided into two different types: the user defined number and the automatically generated number. The user defined numbers are later used in MUFTE for assigning different boundary condition, whereas, the automatically generated numbers are used only in the input file for ART and they start always with zero.

Normally when we deal with fractures they are numbered with negative numbers and the other edges with positive ones.

The executable file for ART is called '*artpoly*'. The command file for ART is called '*default*' and specifies the density of the refinement and gives the possibility to refine the elements of interest. The location of the specific refinement is given in the file '*dens.func*'.

5 NUMERICAL SIMULATIONS

As it has been previously stated, for all the simulations that will be shown here the discrete fracture model concept is being used.
The simulations are divided into two categories: single-phase flow and two-phase flow. Besides, the simulations are further on divided regarding the fracture representation (lower- or equi-dimensional).
In this chapter two kinds of simulations are going to be performed. At first, the implementation of the box-fracture method with regard to the finite element method is being tested for single phase flow in fractured porous media in a two dimensional representation. The same geometry is being later used for the implementation of a two phase flow simulation.
The last example is represented by a 3D geometry that is being used to exemplify the lower dimensional fracture implementation for a two phase flow.

5.1 Single Fluid Phase Flow in Fractured Porous Media: Hydrocoin Level 1 Case 2 (1988) (*Löfman* [2007])

5.1.1 Introduction

In the international hydrologic code intercomparison project (HYDROCOIN) a case with steady-state flow in a two-dimensional slice of a fractured bedrock was considered as Case 2 of Level 1. The case is used to verify the capability of MUFTE code to model heterogeneous flow problems with large permeability contrasts. In addition, the test case is employed to assess the performance of different representations of zones in the finite element mesh. At the same time, the results will be compared with the ones given by the FEFTRA numerical simulator which already showed good results compared to the HYDROCOIN groups.

FEFTRA is a finite element program package developed at VTT for analyses of groundwater flow in site evaluation program that seeks a final repository for spent nuclear fuel in Finland. The code is capable of modeling steady-state or transient groundwater flow, solute transport and heat transfer as coupled or separate phenomena.

As in *Löfman, Vesa & Meszaros* [2007], we represent both rock matrix and fracture zones by 2D elements. This case will address from now on as the *2D fracture model* (see 5.1.6). MUFTE allows elements of different dimensions to be used in the same mesh, i.e. 1D elements for fracture zones and 2D elements for rock matrix (this case will be invoked from now on as *1D fracture model*)

Like MUFTE, FEFTRA code has the capability of combining elements of different dimensionality.

5.1.2 Definition of the problem

The problem is an idealization of the hydrogeological conditions encountered at a potential site for a deep repository in bedrock. The case concerns steady-state flow in a two-dimensional slice of a fractured bedrock intersected by two fracture zones with different widths (10 m and 15 m) and inclinations Figure 9. The fracture zones intersect deep in the modeled 2D cross-section of rock and meet the surface in two valleys. A simple and symmetric topography consisting of straight lines is assumed. The surface near the top corners is horizontal for the first ten meters to define an unambiguous horizontal derivative at the top corners. Flow governed by Darcy's law is influenced by the asymmetry of the fracture zones. Both the zones and the rock matrix are homogeneous and isotropic. The rainfall is assumed to cause the water table to be coincident with the surface. The vertical and bottom boundaries are impermeable to flow.

We considered the origin of the system in the lower left corner of the domain in Figure 9.

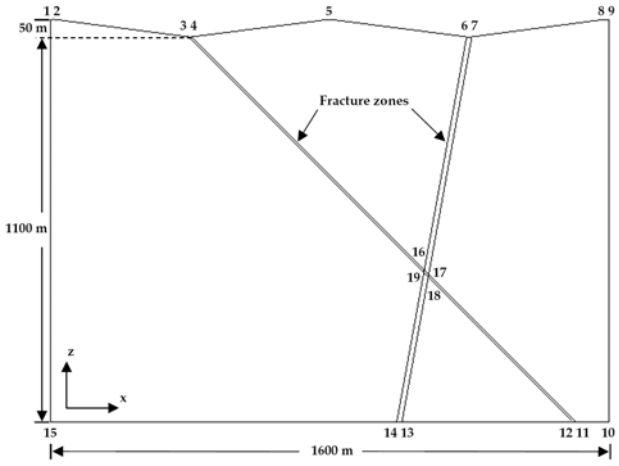

Figure 9: Schematic description of the problem Hydrocoin Level 1 Case 2 (HYDROCOIN 1988). The coordinates of the numbered points are given in Table 1 and

Table 1: Coordinates for 1D fracture model

1D fracture		
Point	x [m]	y [m]
1	0	1150
2	400	1100
3	800	1150
4	1200	1100
5	1600	1150
6	1600	0
7	1500	0
8	1000	0
9	0	0
10	1076.9231	423.0769

Table 2: Coordinates for 2D fracture model

2D fracture		
Point	x [m]	y [m]
1	0	1150
2	10	1150
3	395	1100
4	405	1100
5	800	1150
6	1192.5	1100
7	1207.5	1100
8	1590	1150
9	1600	1150
10	1600	0
11	1505	0
12	1495	0
13	1007.5	0
14	992.5	0
15	0	0
16	1071.35	433.65
17	1084.04	420.96
18	1082.5	412.5
19	1069.81	425.19

5.1.3 Boundary Conditions

The boundary conditions for the one phase one dimensional and two dimensional fracture flow are given in Figure 10 :

1. North Boundary: DIRICHLET Boundary Condition with the hydraulic head h(X,Y) = Y-1000 representing the elevation of the water table.
2. Lateral (X = 0 and X = 1600): NEUMANN (no flow) Boundary Condition
3. Bottom (Y = 0): NEUMANN (no flow) Boundary Condition

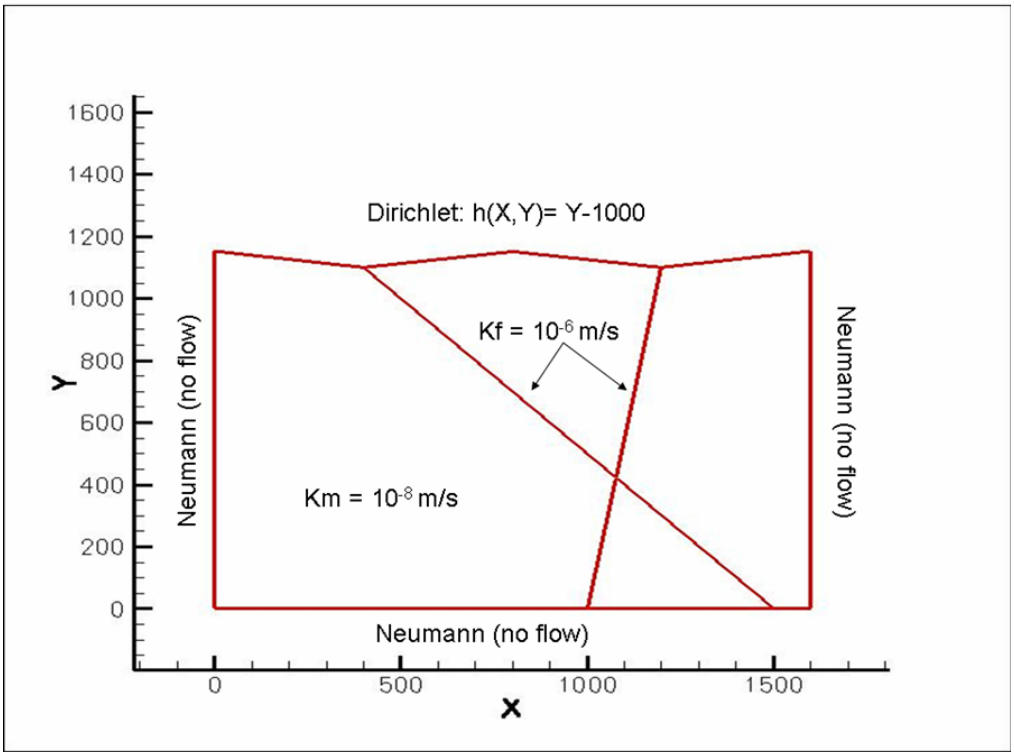

Figure 10: Boundary conditions of the problem Hydrocoin Level 1 Case 2 (HYDROCOIN 1988).

5.1.4 Input parameters. General steps

The input parameters for the 2D model are given in Table 3.

Table 3: Input parameters for the problem Hydrocoin Level 1 Case 2 (HYDROCOIN 1988)

Symbol	Parameter	Value
K_f	Hydraulic conductivity of the fracture zones	1.0×10^{-6} m/s
K_m	Hydraulic conductivity of the matrix zones	1.0×10^{-8} m/s
w_1	Width of fracture 1	10 m
w_2	Width of fracture 2	15 m

The general steps performed were:

1. constructing the geometry by declaring the total number of points, edges and faces
2. discretization of the domain using ART algorithm
3. development of the numerical model in MUFTE
4. application of the numerical model MUFTE and running the simulations using MUFTE-UG
5. extraction of the head distribution at different Y altitudes
6. interpretation of the results

For having a insight into the development of the one phase numerical model in MUFTE (called *k1 problem*) see the Appendix.

5.1.5 1D Fracture Model

The *1D fracture model* case represents the rock matrix using 2D elements and the fracture zones by 1D elements.

The user defined numbers of the data format required by ART in order to generate the refinement (as described in section 4.4.3) are shown in Figure 11. Being a 2D domain the element number is set to zero. As the fractures are elements of lower dimension (1D) and are dealt as inner boundaries when creating the geometry there is no need to define more than one face (which is the entire domain).

The exterior boundaries and fractures are numbered with green color numbers. In order to be able to extract more easily the results at given depths we constructed horizontal inner lines. They are numbered with violet color numbers and when ART is generating the grid these inner lines will facilitate the formation of vertexes on them.

On the left hand side of the graphic are given the altitudes of the lines for the origin of coordinates in the lower left corner. On the right hand side of the graphic are given the altitudes of the inner lines for the coordinate system chosen like in *Löfman, Vesa & Meszaros* [2007].

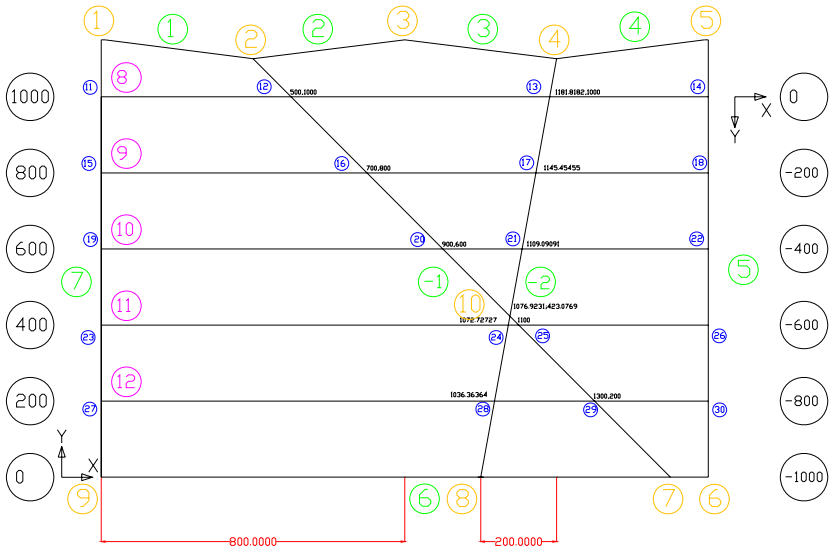

Figure 11: Implementation in ART of the problem Hydrocoin Level 1 Case 2 1D fracture model. Points are numbered with orange and blue color, edges with green (exterior boundaries and fractures) and violet (inner boundaries)

Figure 12 shows the pressure distribution for the 1D fracture model computed using the MUFTE application *k1* (see Appendix).

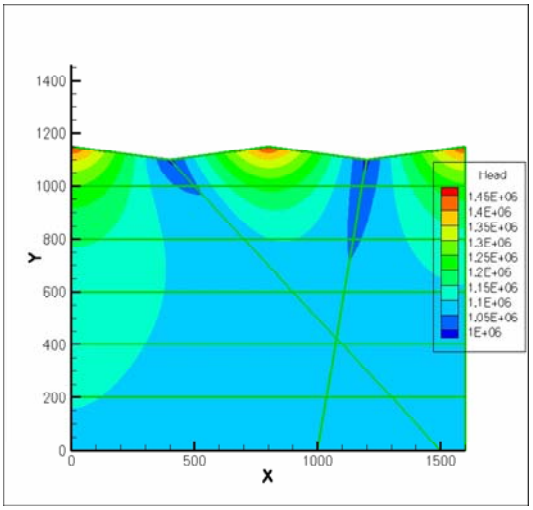

Figure 12: Pressure distribution for 1D fracture model in Hydrocoin Level 1 Case 2 at steady state.

5.1.6 2D Fracture Model

The *2D fracture model* case represents both the rock matrix and the two fracture zones using 2D elements.

Similar to the 1D fracture model the geometry file data input do be discretized with ART is shown in Figure 13. In this case we deal with 9 faces, which are represented by red numbers in squares.

The exterior boundaries and fractures are numbered with green color numbers. In order to facilitate the extraction of the results at given depths horizontal inner lines have been constructed. These lines are numbered with violet color numbers.

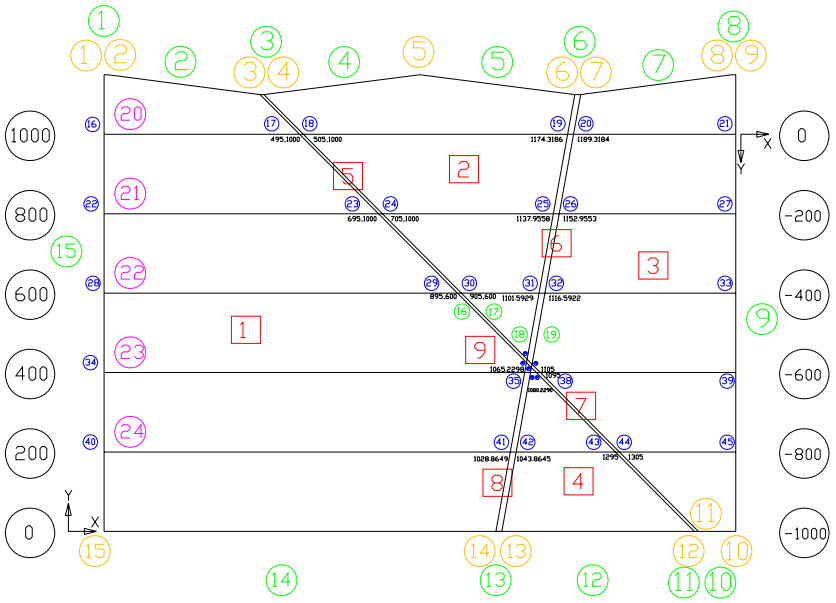

Figure 13: Implementation in ART of the problem Hydrocoin Level 1 Case 2 2D fracture model. Points are numbered with orange and blue color, edges with green (exterior boundaries and fractures) and violet (inner boundaries) and faces with red

The computed pressure distribution for the *2D fracture model* is shown in Figure 14.

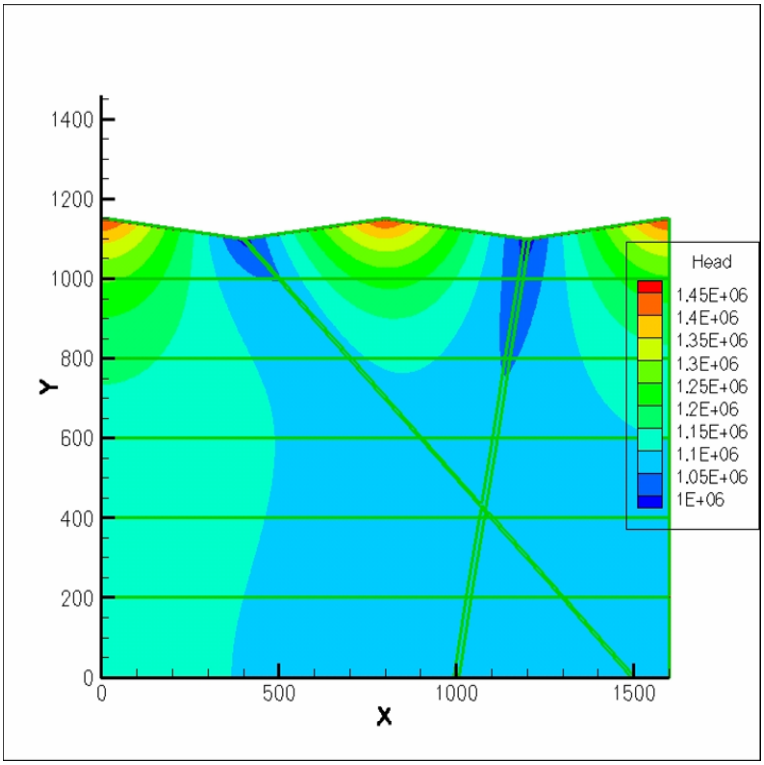

Figure 14: Head distribution for 2D fracture model in Hydrocoin Level 1 Case 2 at steady state.

The Tecplot representations of the permeabilities are plotted in Figure 15. Tecplot is interpolating the values of the absolute permeabilities of fractures and matrix.

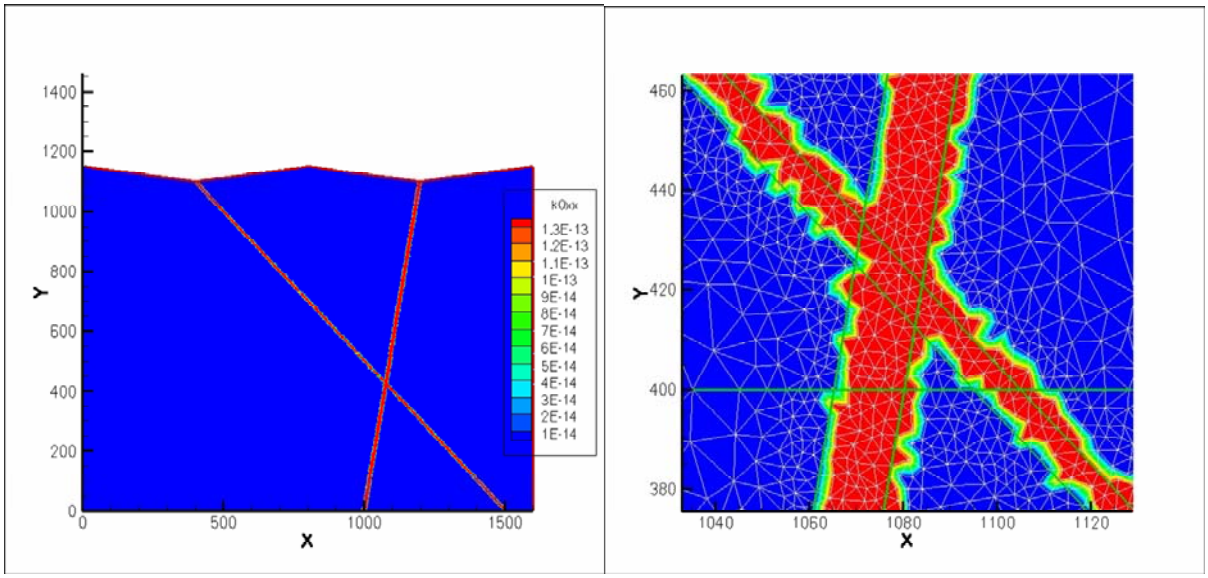

Figure 15: Distribution of the intrinsic permeability in the Hydrocoin Level 1 Case 2 at steady state. Zoom on the two 2D fracture intersection point with their refinement and the permeability distribution according to Tecplot (matrix refinement of 50, fracture refinement 5, resulting in 17293 nodes and 34271 elements)

The ART automatic grid generator was used to compute several grid discretizations. The time necessary for the grid generation is increasing with the increase in the number of elements as Figure 16 shows.

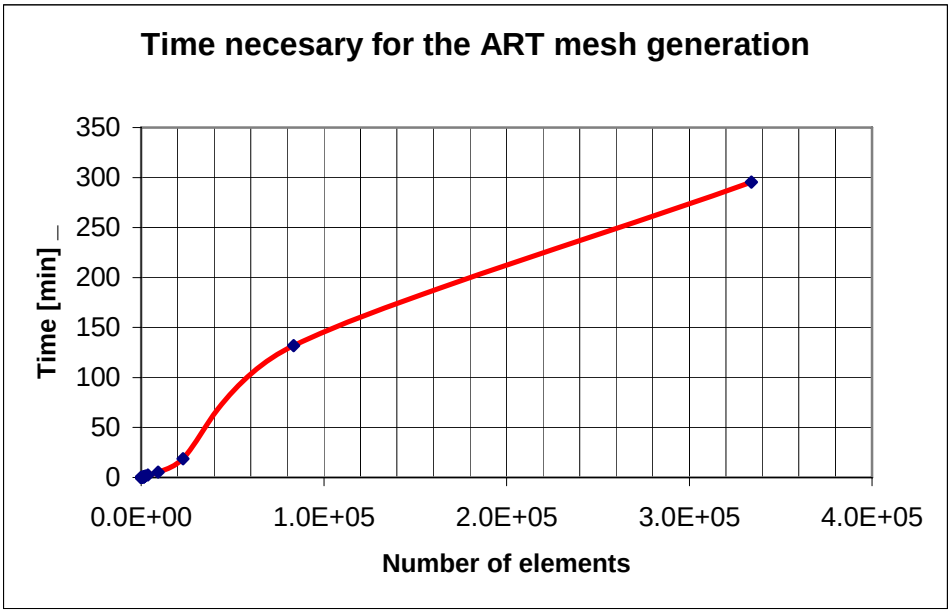

Figure 16: The user time needed to generate in ART the discretizations for the Hydrocoin Level 1 Case 2

5.1.7 Result comparison HYDROCOIN (1988) Level 1 Case 2

Due to the complex geometry finding the analytical solution is almost impossible. For this reason, the results computed with MUFTE-UG were compared to the numerical solutions given by

HYDROCOIN (1988) groups, Grunfelt [1984] and to the ones of Löfman, Vesa & Meszaros [2007] where they used FEFTRA numerical simulator (Figure 18).

However, the comparison with the FEFTRA numerical simulator will be discussed in greater detail in the following.

In order to compare two different numerical simulators one important aspect is to use the same mesh discretization. As the different simulators have certain geometry file formats or even they have their own mesh generating programs, we tried to reproduce the grid discretizations and to have as much as possible the same numbers of element as *Löfman, Vesa & Meszaros* [2007].

Figure 17 shows the 2D mesh in the *1D* and *2D fracture model*, both having the same grid refinement of 37 meters which is very close to the meshes used by *Löfman, Vesa & Meszaros* [2007] in the *base* case (see Figure 18). The elements for rock matrix were approximately of uniform size and the zone elements followed exactly the given geometry.

On the other hand, in Figure 17 can be compared side by side the hydraulic head distributions obtain with MUFTE-UG for the two cases.

Löfman, Vesa & Meszaros [2007] used three different approaches to construct the element mesh as can be seen in Figure 18. In the *base* case, which is similar to our 2D fracture model, both rock matrix and fracture zones were represented by triangular 2D elements.

Like our *1D fracture model*, in the *quadtree* (Figure 18 (b)) and *diagonal* (Figure 18 (c)) cases the elements of different dimensions were used in the same mesh. One thing to keep in mind is to define correctly the thickness of the fractures because the 1D elements have no physical thickness.

The computed hydraulic heads along the horizontal lines are presented in Figure 19 and Figure 20.

The results obtained with MUFTE for *1D fracture model* are nearly identical to the ones computed with FEFTRA for the *quadtree* and *diagonal* case.

For 2D fracture model the results obtained are nearly identical to the base case in FEFTRA and to Grunfelt (1984).

The 1D fracture model gives slightly lower heads than the 2D fracture model especially deeper in the bedrock (Y=200m). One explanation is that when fractures are simulated as 1D elements there is a small error introduced because the physical space is taken by rock matrix and receives the rock matrix properties. It means that in this case we have another 10 meters for the first fracture, respectively 15 meters, for the second that become rock matrix.

One important difference between MUFTE-UG simulator and FEFTRA is the numerical scheme utilized for solving the partial differential equations. The FEFTRA group solved the partial differential equations describing groundwater flow employing the conventional Galerkin technique (*Huyakorn* and *Pinder* [1983]) while in my model was used the vertex centered finite volume

scheme. The matrix equation resulting from the finite element formulation was solved employing the conjugate-gradient method (*Atkinson* [1988]). The flow paths (in 3D cases only) were computed with the algorithm that uses the continuous Darcy velocity field obtained by treating q as an unknown variable and applying the finite element method (*Yeh* [1981])

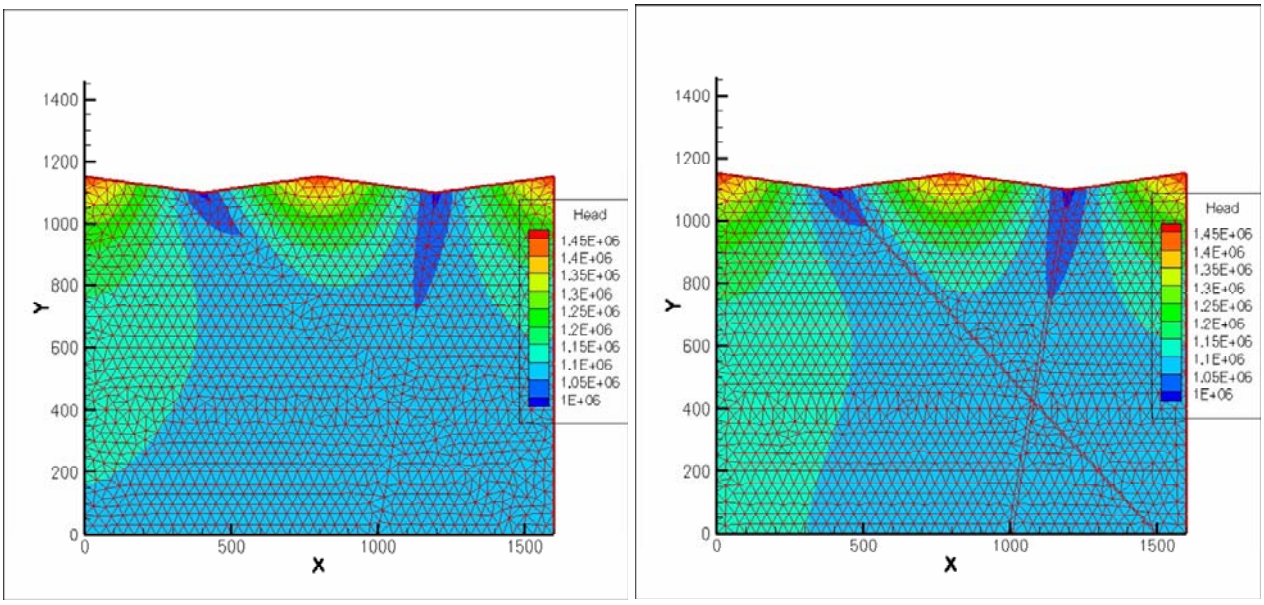

a) **b)**

Figure 17: Finite element meshes and pressure distribution for a) 1D fracture model (1559 nodes, 2966 elements) and b) 2D fracture model (1662 nodes, 3164 elements)

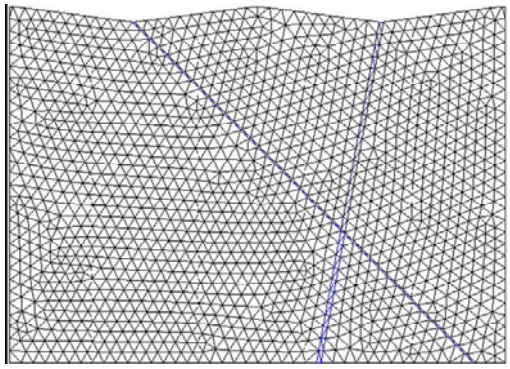

a) base case (1554 nodes, 2957 elements)

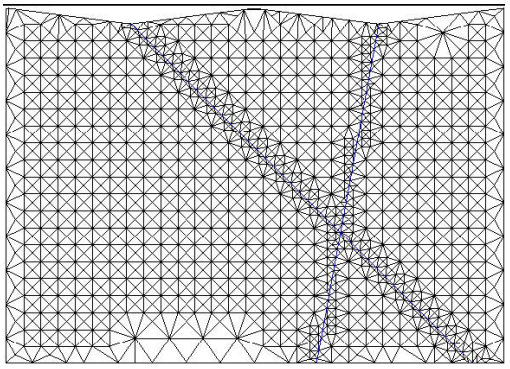

b) quadtree case (1450 nodes, 2940 elements)

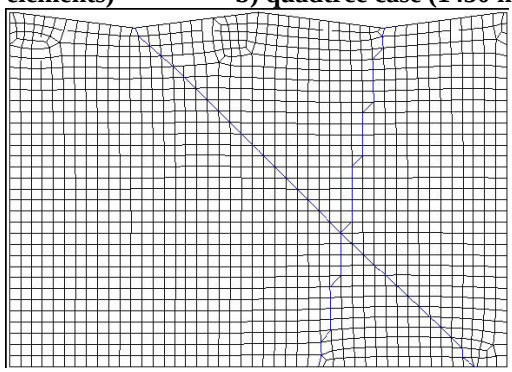

c) diagonal case (1537 nodes, 1520 elements)

Figure 18: Finite element meshes for the problem Hydrocoin (1988) Level 1 Case 2 used in FEFTRA numerical simulation from Löfman, Vesa & Meszaros [2007].

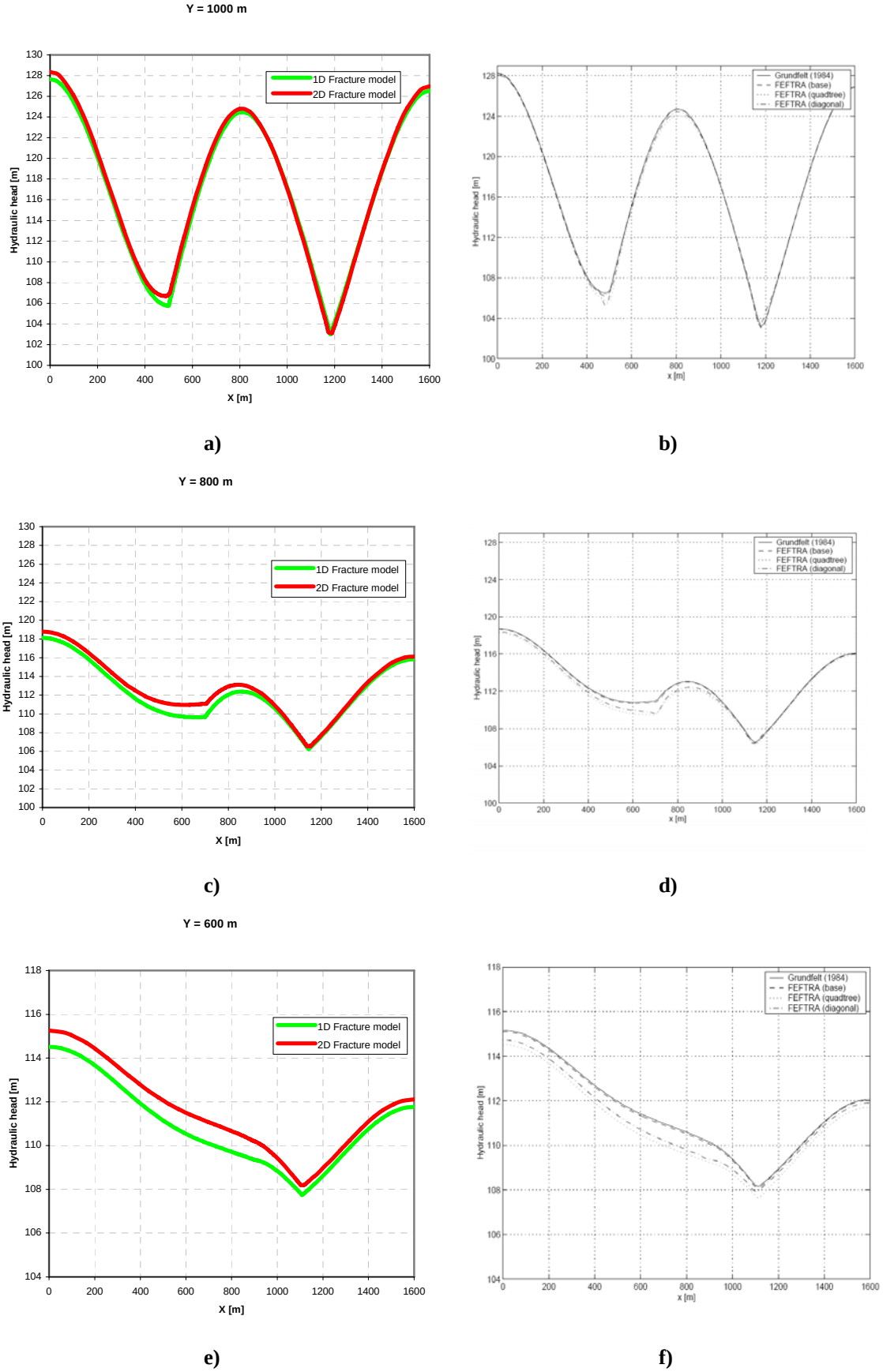

Figure 19: Comparison of the computed hydraulic heads along horizontal lines. The results computed by MUFTE-UG are presented in subfigures a), c), e) whereas subfigures b), d), f) present the heads computed by FEFTRA and Grundfelt (1984)

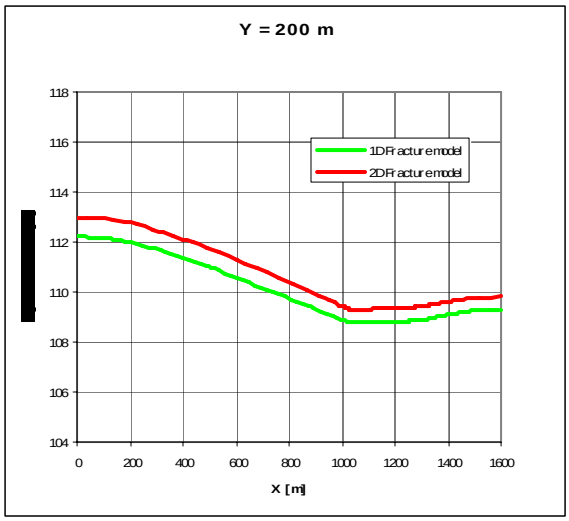

a)

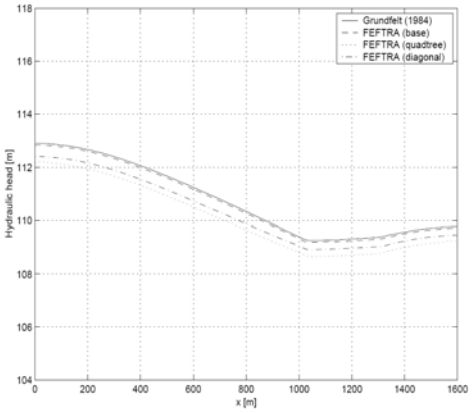

b)

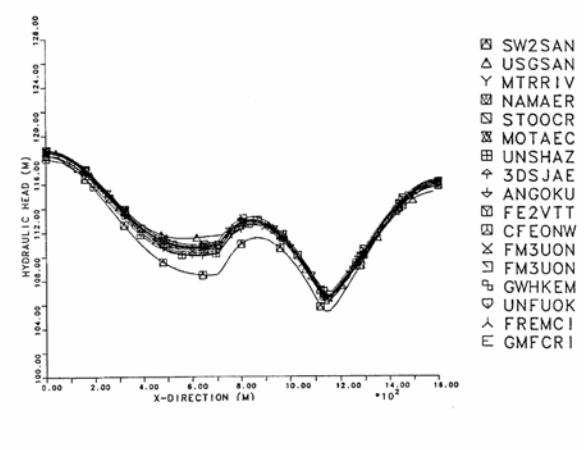

c)

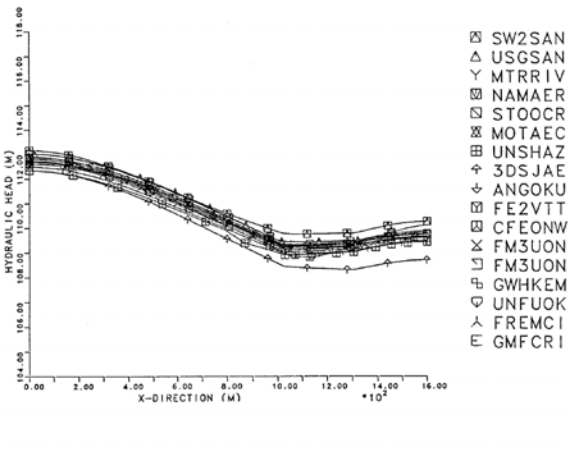

d)

Figure 20: Comparison of the computed hydraulic heads along horizontal lines. Subfigure a) presents the results computed by MUFTE-UG, subfigure b) presents the results computed by FEFTRA and Grunfelt (1984) and subfigures c) and d) show the heads computed by the HYDROCOIN (1988) groups with the finest meshes.

After comparing the hydraulic heads another comparison performed was for the flow paths.

One important feature of Tecplot is to allow the computation of the trajectories of massless particles in a steady-state velocity field. These trajectories are called streamtraces.

Taking advantage of this feature by using the Darcy X and Darcy Y flow components the pathlines were plotted for the two cases: *1D* and *2D fracture model* (Figure 21, Figure 22).

The flow path passing through (X = 100 m, Y = 800 m) is used as reference for comparison with FEFTRA and with the HYDROCOIN (1988) results.

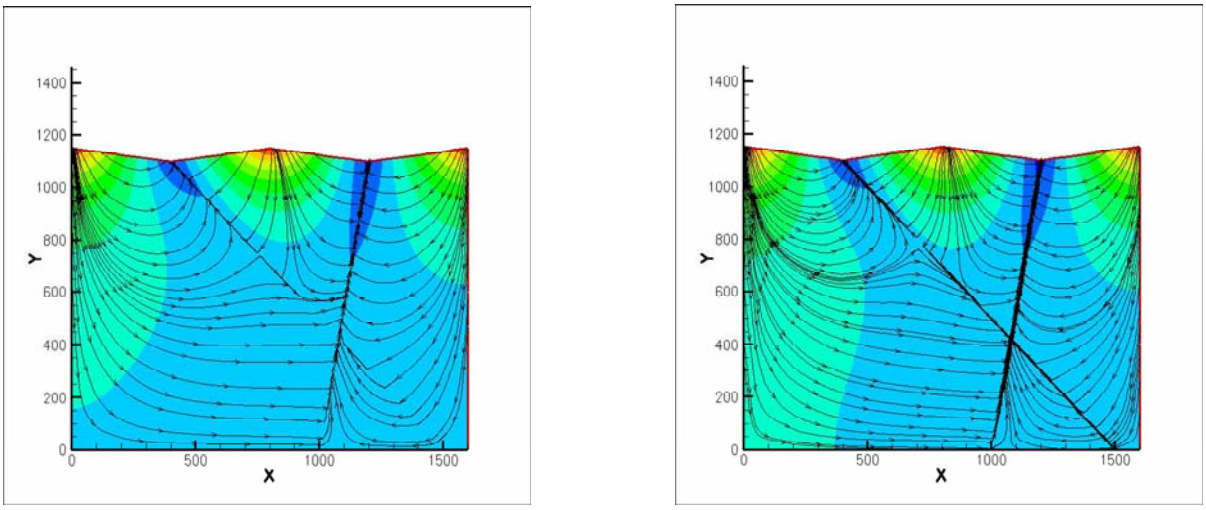

a) **b)**

Figure 21: Path lines (streamtraces) in the modeled region of a) 1D fracture model ; b) 2D fracture model

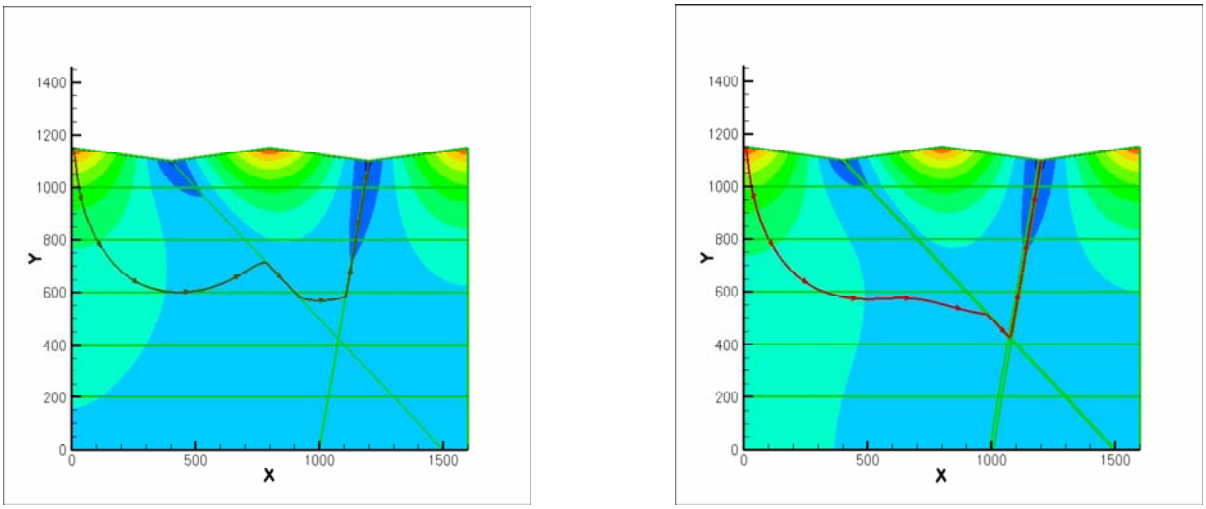

a) **b)**

Figure 22: Path lines passing through the point (X=100 m; Y = 800 m) for a) 1D fracture model b) 2D fracture model

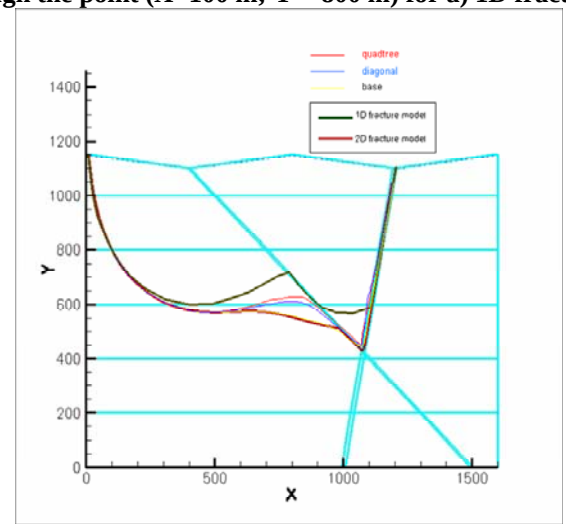

Figure 23: Path lines passing through (X = 100, Y=800) for the *1D* and *2D fracture model* computed with MUFTE-UG and for *quadtree*, *diagonal* and *base* cases computed with FEFTRA

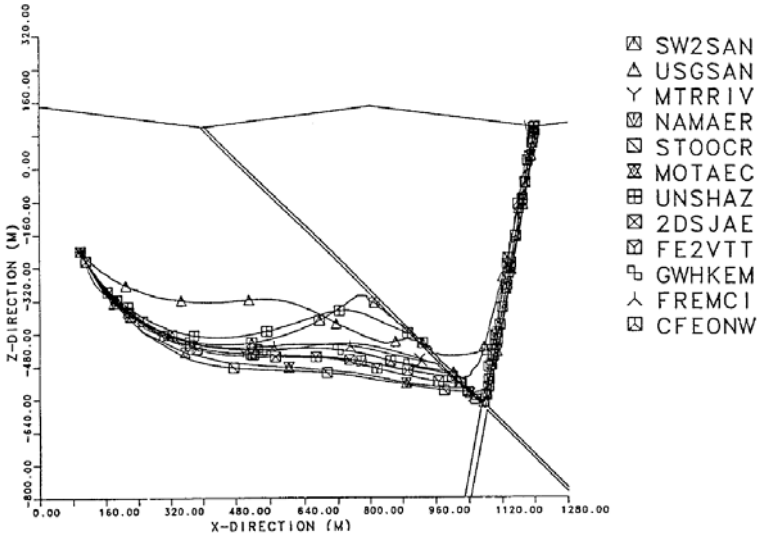

Figure 24: Flow path by the HYDROCOIN (1988) groups

The comparison of MUFTE to FEFTRA results and to the analytical, semianalytical and/or other numerical solutions proves the capability of MUFTE to simulate such problems.

5.1.8 Grid Convergence Test

Simulations with too coarse grids result in numerical diffusion but on the other hand simulations with very fine grids require longer computational time. Therefore, a grid convergence test is necessary to decide which grid size is acceptable considering the amount of numerical diffusion.

Several grid discretizations were tested. The discretizations are listed in Table 4 for *1D fracture model* and Table 5 for *2D fracture model* together with the time necessary for generating them, their number of vertexes, edges and elements, and the corresponding refinement.

The last columns of the table exhibit the time required to run the MUFTE-UG with the respective geometry discretization.

To run these simulations a Pentium III (Coppermine) processor with 1 GHz and a 512 MB RAM memory were used.

The real time – is the elapsed time from the beginning to the end of the program.

However, the CPU time is divided into user and sys. The user value is the time used by the program itself and any library subroutines it calls. The sys value is the time used by system calls invoked by the program. (directly or indirectly)

The sum of user+sys is the total direct CPU cost of executing the program. This does not include the CPU costs of parts of the kernel that can be said to run on behalf of the program, but which do not actually run on its thread.

Table 4: Discretization and computation for 1D fracture model

Name of the ART file	Matrix Refinement [m]	Fracture Refinement [m]	Artmesh Time [min]	Vertex Number	Edge Number	Face Number	Computational time MUFTE [min]					
							real		user		sys	
							min	sec	min	sec	min	sec
q.net_1Df_500_r000	500	0	0.006667	34	79	46	**0**	35.1	**0**	1.93	**0**	0.826
q.net_1Df_500_r100	500	100		492	1414	923	**0**	35.7	**0**	9.641	**0**	0.363
q.net_1Df_500_r050	500	50		992	2896	1905	**1**	12.1	**0**	23.151	**0**	0.971
q.net_1Df_400_r000	400	0	0.031833	39	93	55	**0**	23.7	**0**	1.278	**0**	0.288
q.net_1Df_400_r100	400	100		662	1907	1246	**0**	39.5	**0**	13.207	**0**	0.412
q.net_1Df_400_r050	400	50		1246	3643	2398	**1**	3.2	**0**	33.37	**0**	0.468
q.net_1Df_300_r000	300	0	0.0315	52	130	79	**0**	22.8	**0**	1.103	**0**	0.231
q.net_1Df_200_r000	200	0	0.031833	69	176	108	**0**	23.8	**0**	1.224	**0**	0.222
q.net_1Df_100_r000	100	0	0.135667	263	730	468	**0**	39.3	**0**	4.836	**0**	0.36
q.net_1Df_075_r000	75	0	0.161	441	1239	799	**0**	43.1	**0**	7.606	**0**	0.36
q.net_1Df_050_r000	50	0	0.561167	924	2653	1730	**0**	54.1	**0**	16.844	**0**	0.427
q.net_1Df_050_r005	50	5	17.4968	14389	42879	28491	**184**					
q.net_1Df_050_r003	50	3	60.5828	27294	81585	54292	**1229**	13.7	**1207**	43.801	**1**	26.7
q.net_1Df_045_r015	45	15	11.9823	7045	20801	13757						
q.net_1Df_040_r000	40	0	0.697667	1359	3936	2578						
q.net_1Df_0375_r000	37.5	0	0.748167	1514	4396	2883						
q.net_1Df_037_r000	37	0	0.493167	1559	4524	2966	**1**	7.94	**0**	30.349	**0**	0.83
q.net_1Df_035_r000	35	0	1.03	1753	5097	3345						
q.net_1Df_030_r000	30	0	1.4895	2337	6823	4487	**1**	31.9	**0**	53.742	**0**	0.537
q.net_1Df_025_r000	25	0	2.45367	3756	11034	7279	**2**	46.9	**1**	56.112	**0**	0.664
q.net_1Df_015_r000	15	0	5.56417	9354	27681	18328	**9**	13.6	**7**	56.525	**0**	1.57
q.net_1Df_015_r005	15	5	104.041	51799	154466	102668						
q.net_1Df_010_r000	10	0	18.9512	22932	68194	45263	**80**	36.3	**76**	17.898	**0**	5.313
q.net_1Df_005_r000	5	0	131.733	83491	249333	165843	**949**	22.3	**783**	22.479	**5**	44.2
q.net_1Df_0025	2.5	0	295.375	334053	999840	665788						

Table 5: Discretization and computation for 2D fracture model

Name	Matrix Refinement	Fracture Refinement	Artmesh Time [min]	Vertex Number	Edge Number	Face Number	Computational time MUFTE [min]					
							real		user		sys	
							min	sec	min	sec	min	sec
q.net_2Df1000_300_r010	300	0	0.0721667	77	199	123	**0**	21.587	**0**	0.983	**0**	0.239
q.net_2Df1000_200_r000	200	0	0.07483	97	254	158	**0**	21.154	**0**	1.074	**0**	0.231
q.net_2Df1000_200_r010	200	10	13.5972	8685	25873	17189	**8**	45.732	**7**	8.935	**0**	1.93
q.net_2Df1000_150_r010	150	0	0.0761667	145	390	246						
q.net_2Df1000_100_r010	100	0	0.136667	283	781	499	**0**	22.765	**0**	2.145	**0**	0.221
q.net_2Df1000_075_r010	75	0	0.24	489	1378	890	**0**	19.389	**0**	3.327	**0**	0.204
q.net_2Df1000_050_r005	50	5	27.3075	17293	51563	34271						
q.net_2Df1000_050_r003	50	3	91.4327	41255	123422	82168						
q.net_2Df1000_050_r000	50	0	0.4365	968	2781	1814	**0**	24.524	**0**	6.081	**0**	0.245
q.net_2Df1000_037_r000	37	0	2.10733	1662	4825	3164	**0**	31.315	**0**	10.436	**0**	0.318
q.net_2Df1000_030_r000	30	0	2.26183	2433	7100	4668						
q.net_2Df1000_025_r000	25	0	3.32217	3481	10210	6730	**0**	57.551	**0**	24.512	**0**	0.507
q.net_2Df1000_010_r000	10	0	14.6425	20896	62115	41220	**11**	31.343	**8**	24.127	**0**	2.779
q.net_2Df1000_005_r000	5	0	138.323	83810	250268	166459	**138**	31.888	**102**	49.333	**0**	44.187

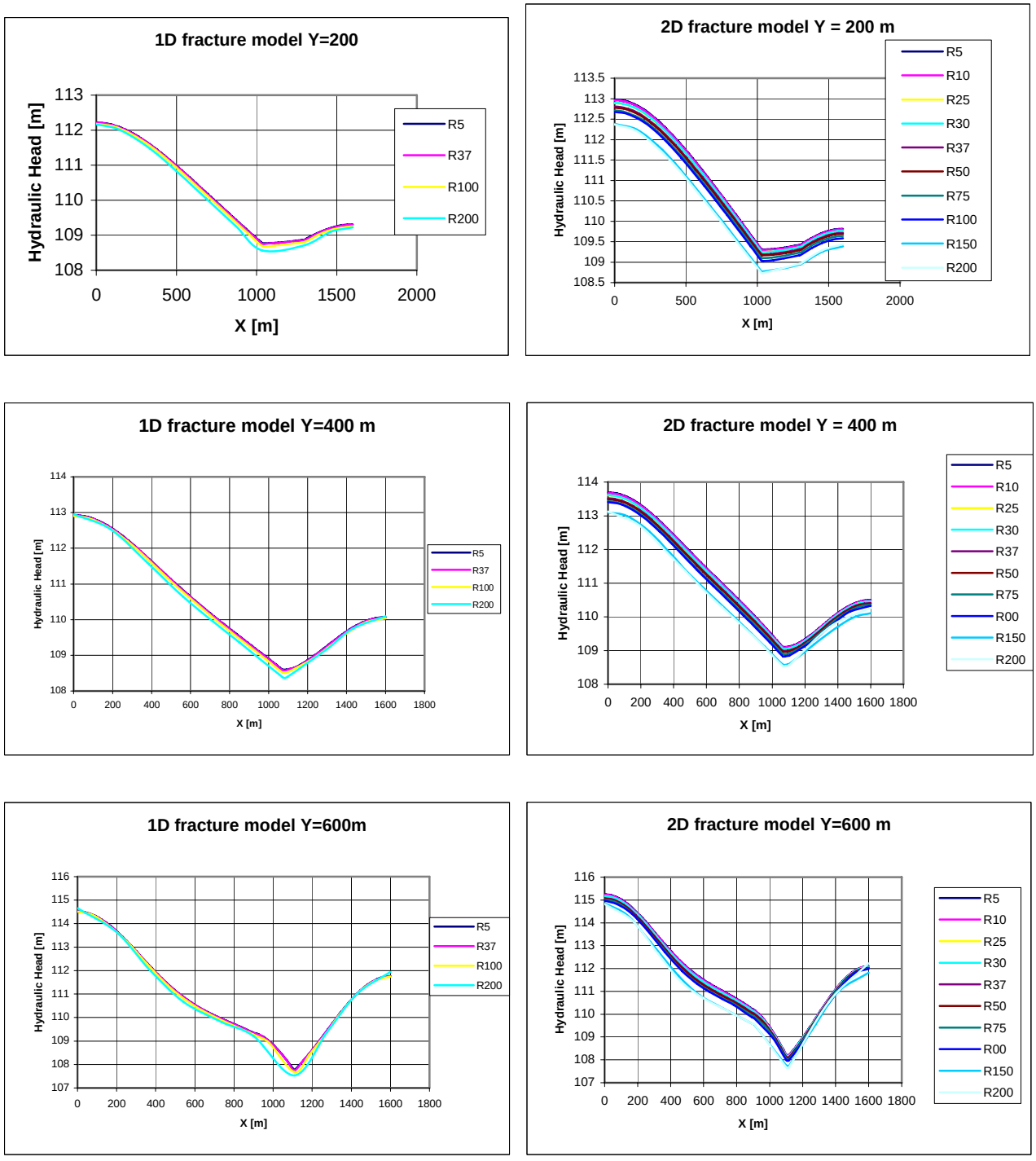

Figure 25: Computed hydraulic heads along horizontal lines for different grid refinements (i.e. R37) showing the grid convergence

5.1.9 Computation Time

The two different fracture models computed with MUFTE-UG require different computation times as shown in Figure 26. The *1D fracture model* seems to require more time. This can be interpreted that the box fracture algorithm utilized in the *1D fracture model* requires more time than the simple box method in *2D fracture model.*

For the case of one phase flow to apply a less dimensional fracture is not necessarily leading to an improve in computation time.

Nevertheless, by using a less dimensional discrete fracture approach we will always need less number of elements to represent the fracture correctly and consequently we will have a faster computation.

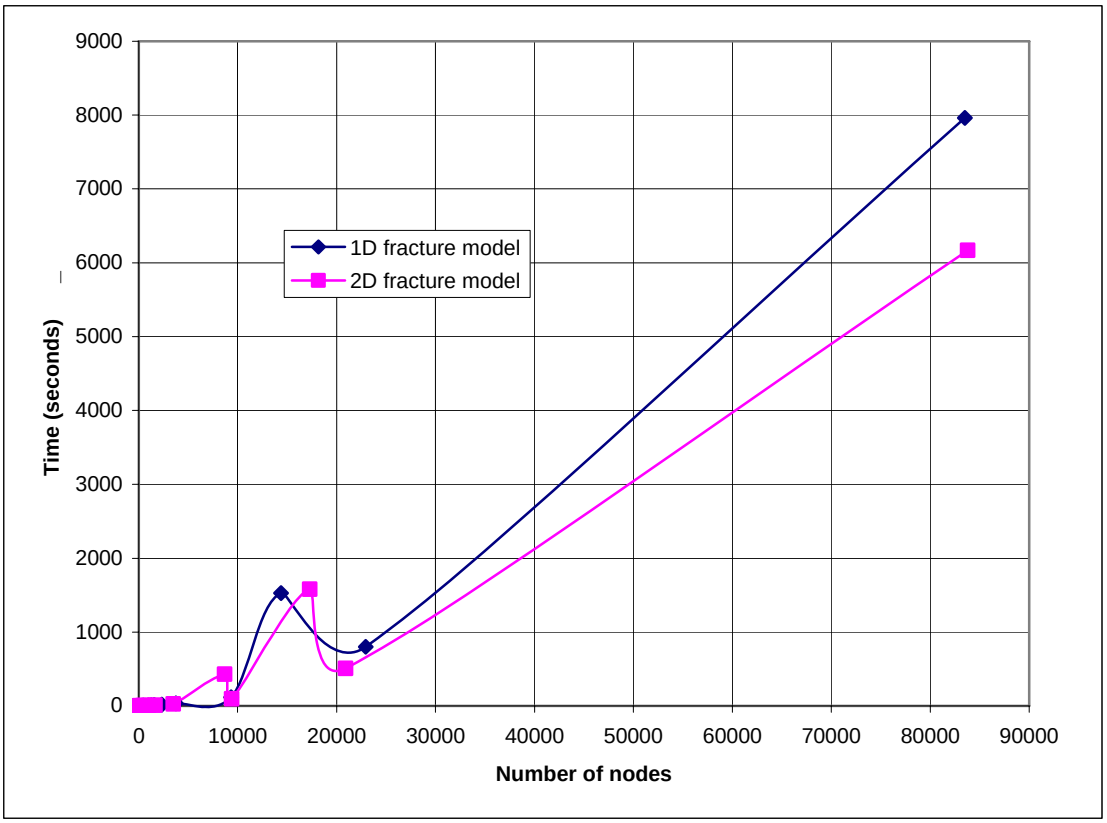

Figure 26: Computation time for 1D and 2D fracture models using MUFTE-UG as a function of number of nodes

5.2 Two Fluid Phase Flow in Fractured Porous Media

To demonstrate the capability of the numerical simulator MUFTE-UG we develop a two fluid phase problem first in a 2D domain and than in a 3D domain.

5.2.1 2D Domain for Two Fluid Phase Flow in Fractured Porous Media: Hydrocoin Level 1 Case 2 (1988) Geometry

The purpose of the first numerical experiment for the two phase fracture-flow is to asses the difference between a lower- and an equi-dimensional fracture approach. The same geometry as used in the one phase-flow simulation is set up. (see section 5.1.2)

Similar to the one phase flow, the rock matrix is represented by 2D elements and the fracture by 1D elements.

The boundary conditions for the two phase fracture flow in two-dimensional domain are represented in Figure 27.

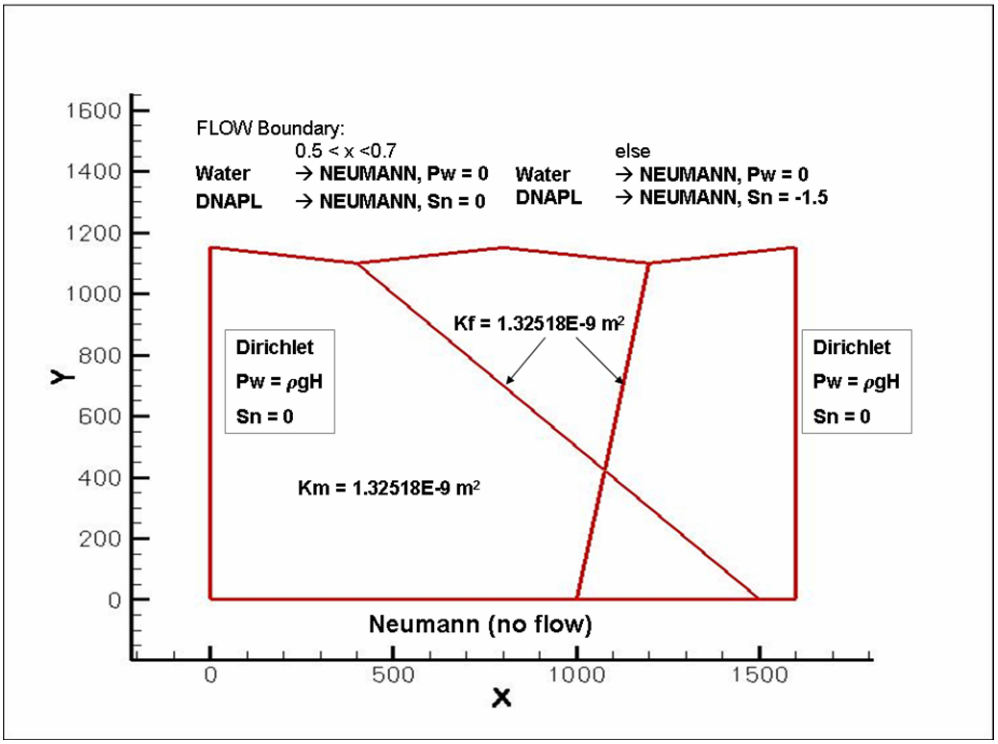

Figure 27: Boundary conditions for the two phase fluid flow problem on Hydrocoin Level 1 Case 2 geometry

The input parameters for the two media, matrix and fracture, and for the two fluid phases are given in Table 6 and Table 7. The capillary pressure function given in the Brooks-Corey and Van Genchten formulations is shown in Figure 28. The two phase parameters of the simulation are artificially chosen but give a representative picture of the fracture-matrix interaction.

Table 6: Input parameters for the two phase fracture-flow problem in 2D domain

	matrix	*fracture*
BC lambda	3.5	2
BC Pd	1000	200
Swr	0.08	0.05
Snr	0	0
VG_alpha	0.00085	0.0037
VG_n	5.65	4.7
Porosity	0.4	0.4
Abs. permeability	1.32518E-13	1.32518E-09

Table 7: The two fluid properties for the fracture-flow problem in 2D domain

	Water	**DNAPL**
Density [kg/m^3]	1000	1600
Dyn. Viscosity [kg/m.s]	1.00E-03	5.70E-03

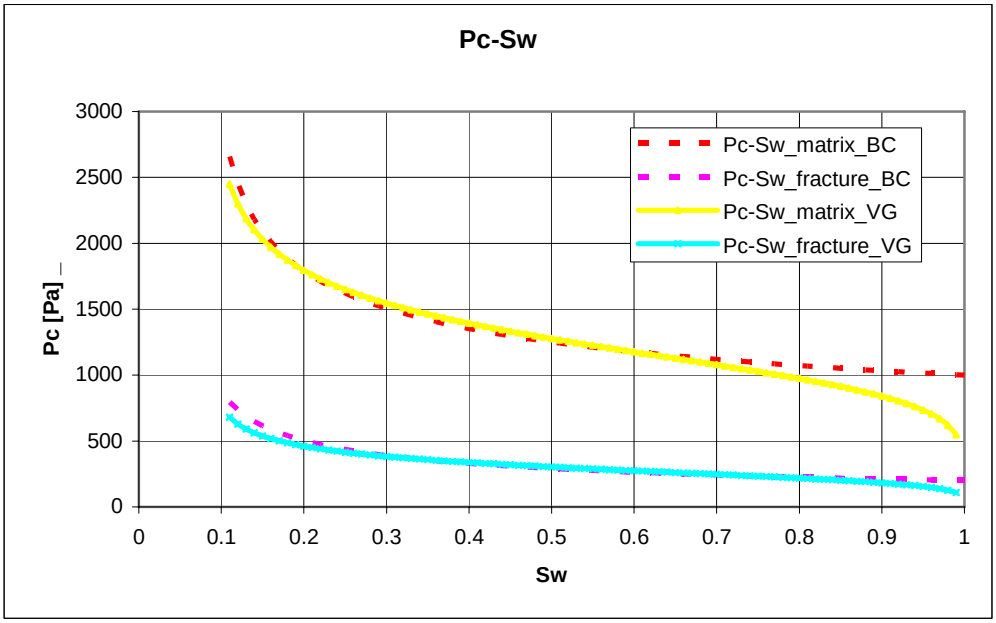

Figure 28: Capillary pressure functions after Brooks Corey and Van Genuchten for Hydrocoin Level 1 Case 2 geometry in two phase flow problem

It has to be reminded that, for all cases, the porosity of both materials (fracture and matrix) is equal to 0.4.

We compared the results obtained with different formulations of the capillary pressure (Brooks-Corey and Van Genuchten) and in the same time we investigated the influence of the fracture absolute permeability on the saturation front movement. The permeability values given in Table 6 are considered as initial values and will be used to compare the results obtained with the two capillary pressure- saturation formulations. For the *1D fracture model* was conducted a simulation for comparing the influence of the fracture width on the non-wetting saturation front.

During the simulations I vary only one parameter at the time and keep the other constant.

For, both the*1D* and *2D fracture model* for two phase flow simulation I employed a mesh discretization generated with ART (see section 4.4.3) with a constant refinement of 30 m.
The vertex-centered finite volume scheme or the box scheme was used to calculate the flow equations. For the simulation we employ the backward Euler scheme with fixed time step size. The nonlinear equations are solved by inexact Newton linearization. The solver used to solve the inexact Newton algorithm is the Bi-Conjugate Gradient Stabilized solver (Bi-CGSTAB) (see *Bastian* [1999]).
In each Newton step a defect reduction of 1.0E-10 is prescribed and a linear defect reduction of 1.0E-05.

For the two phase flow simulation we didn't investigate the influence of the discretization length on the performance.
As in the case of the one-fluid phase fracture flow Hydrocoin Level 1 Case 2 (see section 5.1) this numerical simulation was developed in several steps:

1. constructing the geometry by declaring the total number of points, edges and faces
2. discretization of the domain using ART algorithm
3. development of the numerical model in MUFTE
4. application of the numerical model MUFTE and running the simulations using MUFTE-UG
5. extraction of the saturation distribution
6. interpretation of the results

The geometry construction (step 1, 2) are the same as in the one-phase flow (see section 5.1). Step 3, the development of the numerical model, would take too much to detail in the space of this study.

5.2.1.1 Comparison BC and VG Formulations in the 2D Fracture Model

First, we compare the Brooks-Corey (BC) and Van Genuchten (VG) formulations for capillary pressure – saturation formulation using the parameters in Table 6. We see that there is a good agreement between the two formulations (Figure 29). Here only the results for the *2D fracture model* will be presented while for the *1D fracture model* we get the same positive agreement.

5.2.1.2 Influence of the Absolute Permeability in Fractures on the Saturation Distribution

The second numerical experiment is to assess the effect of the fracture permeability on the non-wetting saturation front. The results are plotted for the *2D fracture model* and can be seen in Figure 30.

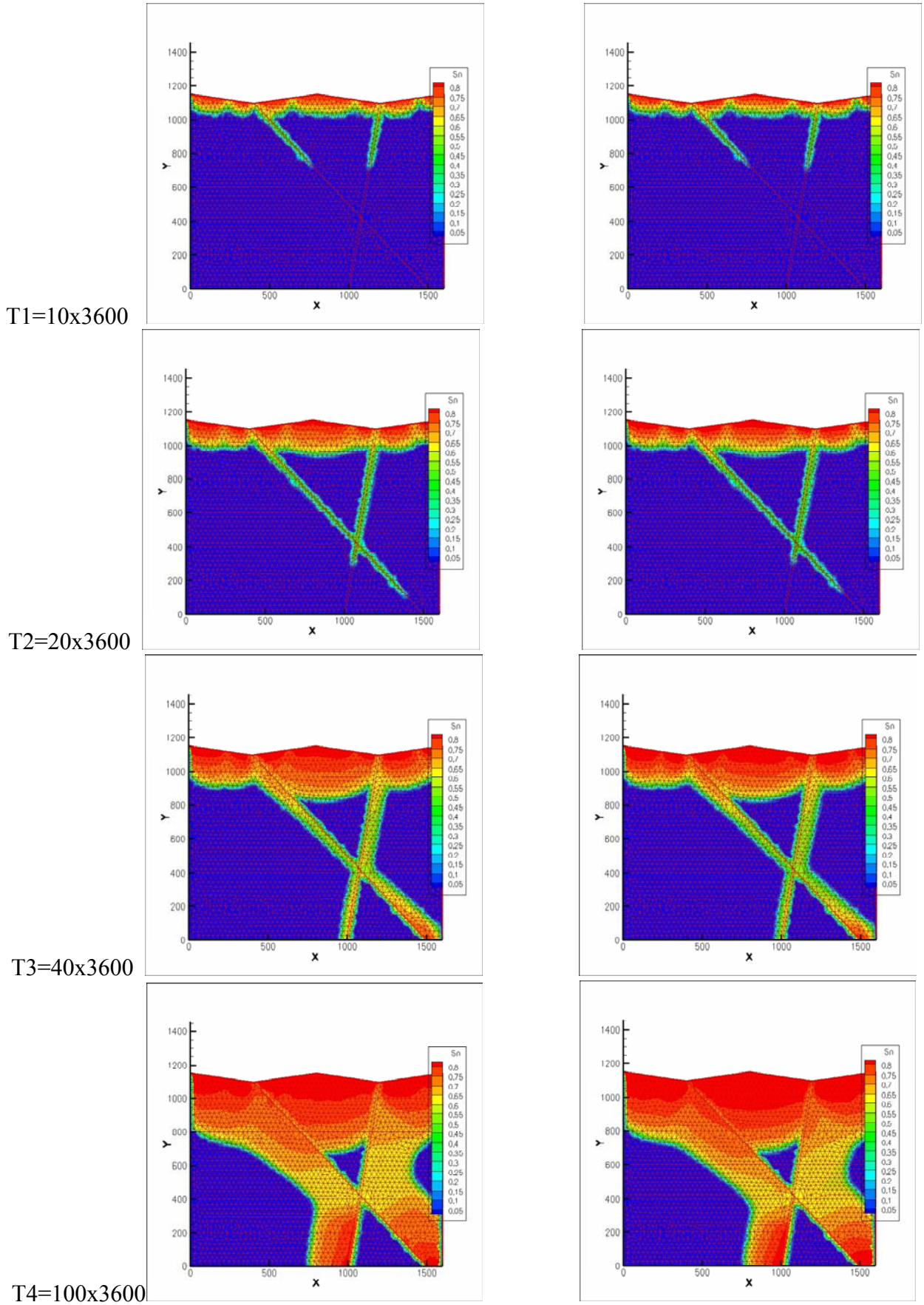

a) Brooks Corey formulation **b) Van Genuchten formulation**

Figure 29: Comparison between the DNAPL saturation front s for 2 phase flow in the 2D fracture model for a) Brooks-Corey formulation and b) Van Genuchten formulation for time steps T1, T2, T3 and T4

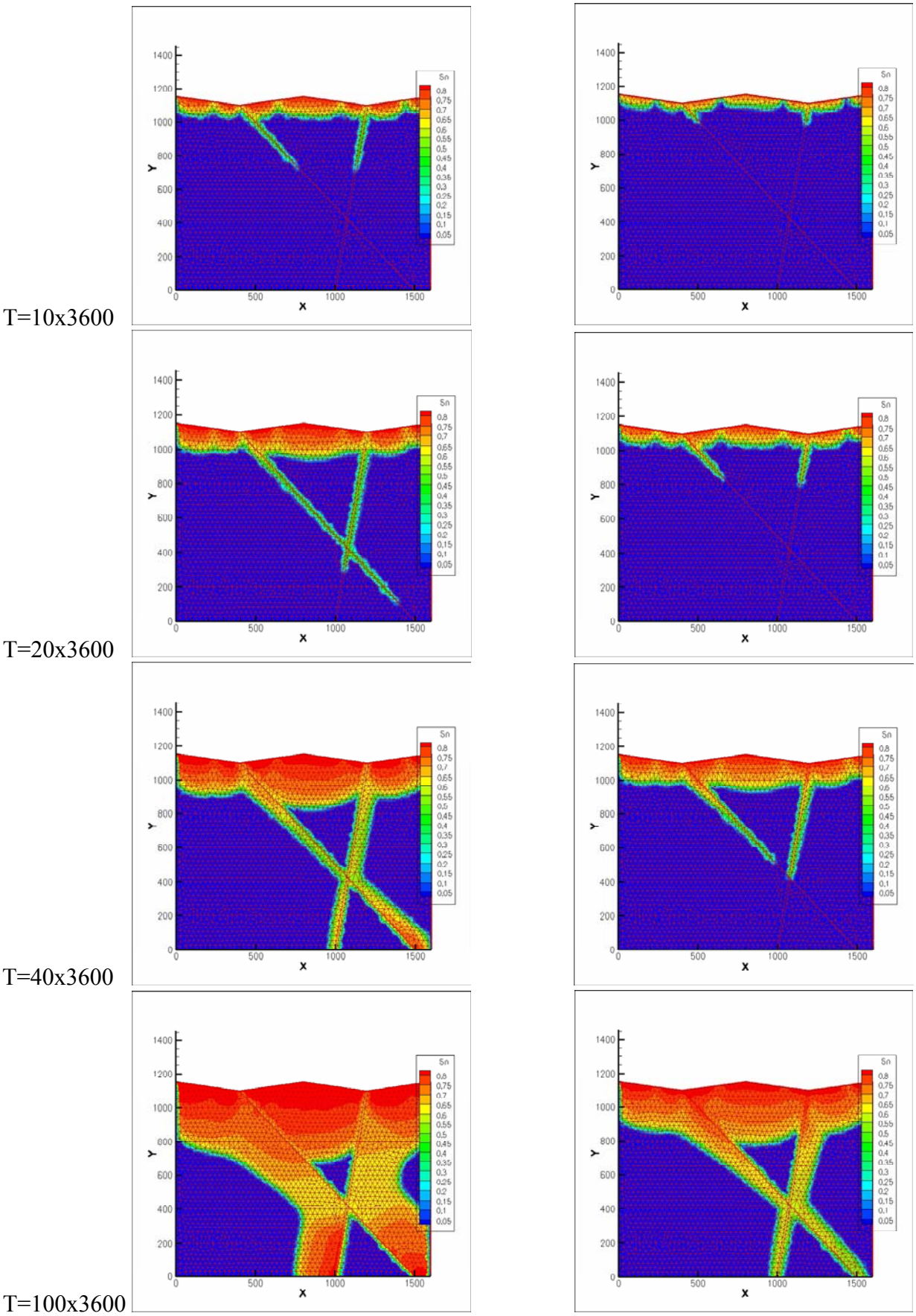

Figure 30: Comparison between the DNAPL saturation fronts for 2 phase flow in the 2D fracture model for a constant matrix permeability Km = 1.33E-13 and tow different fracture permeabilities a) Kf1 = 1.33E-10 and b) Kf2 = 1.33E-10 for T1= 10*3600 s; T2= 20*3600 s; T3= 40*3600 s and T4= 100*3600 s;

The first value of the fracture's intrinsic permeability is Kf1 = 1.32518E-09 and the second one is Kf2 = 1.32518E-10.

5.2.1.3 Comparison 1D and 2D fracture model

Considering a Van Genuchten formulation for the capillary pressure-saturation relationship (see Table 6) I compare the *1D* and the *2D fracture model* for two phase flow (Figure 32).

In Figure 31 it is displayed the shape of the saturation curve for the two models at time T=100x3600 s by making a cut at Y = 600 m. This is a very interesting comparison since the mixed-dimensional model (*1D fracture model*) is evaluated with a "trusted one", the model with two-dimensional elements (*2D fracture model*).

When examining the mass of the system, it is known that this is the same for both realizations. A contradicting impression could arise because the saturation curve for the *1D fracture model* seems to comprise less mass. The differences are however small. The causes for this my be in the upper boundary line definition which is not considering the 10 m and respectively 15 m of the fracture width in the 1D. Also the fracture width in the 1D model is taken by matrix property.

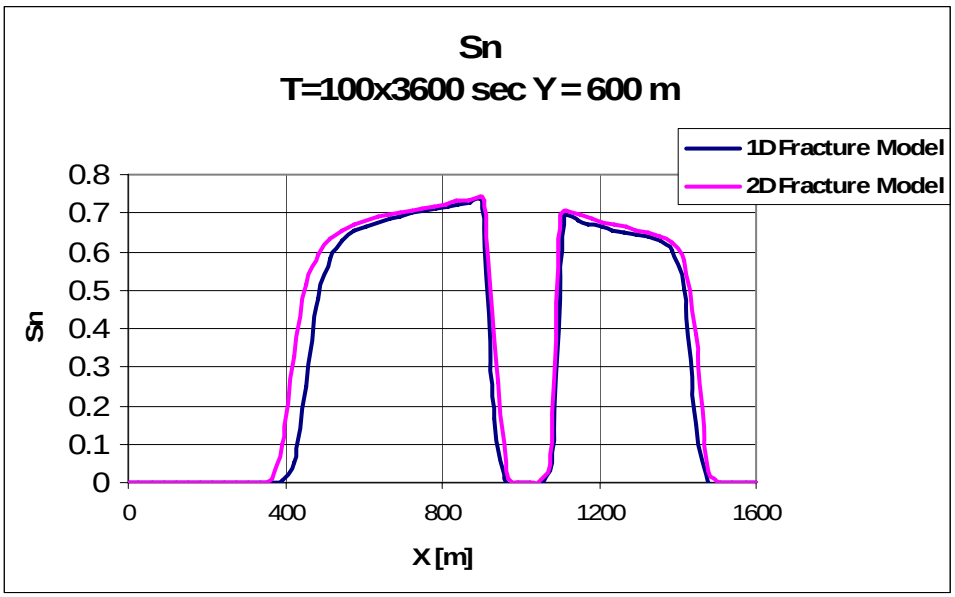

Figure 31: DNAPL saturation at Y=600m and T = 100x3600 for 1D and 2D fracture model for a Van Genuchten capillary pressure formulation.

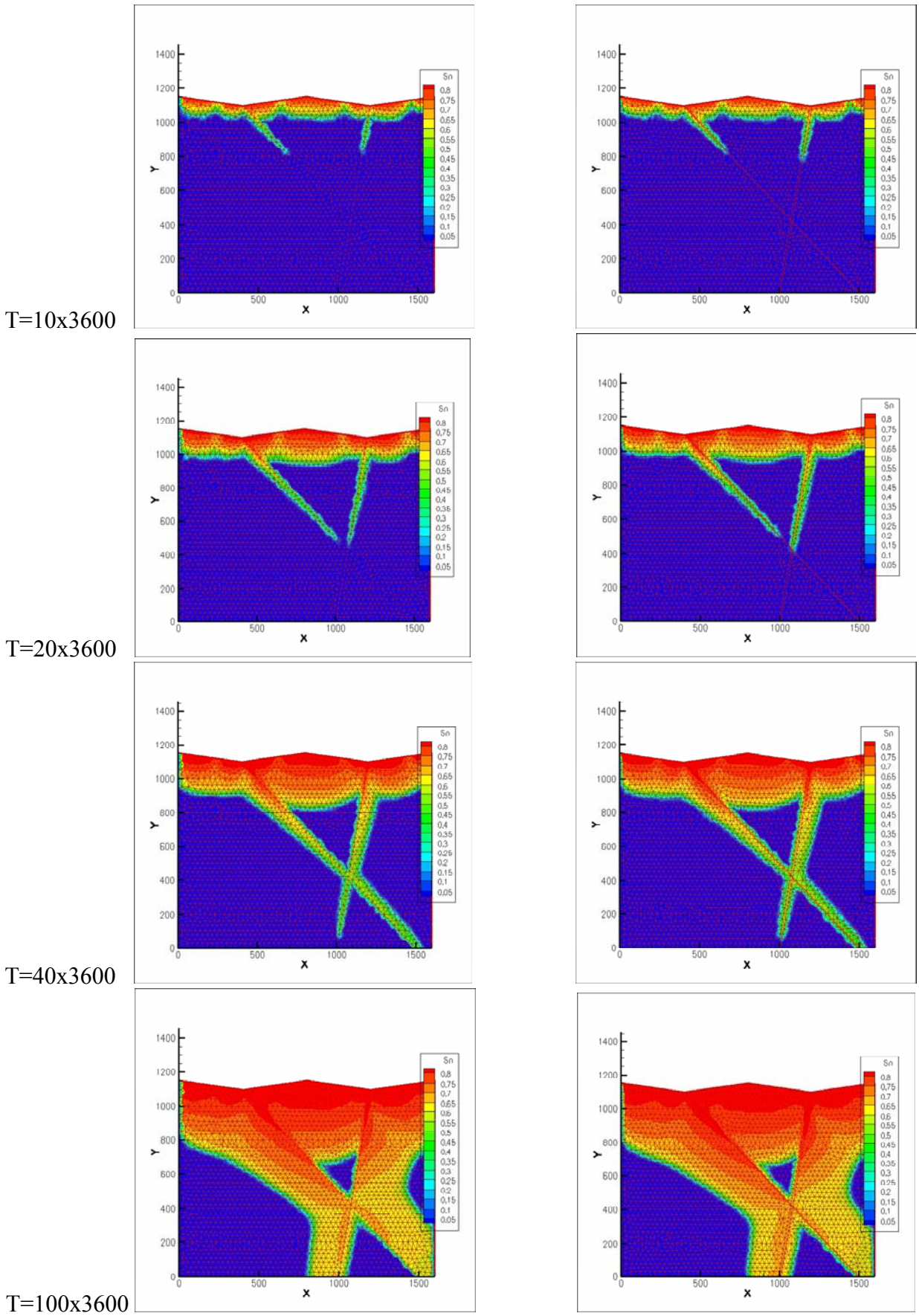

Figure 32: Saturation comparison between 1D and 2D fracture models for two phase flow using at given time steps and using a Van Genuchten capillary pressure –saturation formulation.

5.2.1.4 Influence of the fracture width in the 1D Fracture Model

In this section we will investigate the influence of the fracture width in the lower-dimensional representation of fractures. In Figure 34 the saturation fronts are plotted at given time intervals (T1 = 20x3600sec; T2=40x3600sec; T3=100x3600sec). The fronts are compared two by two on the same scale of saturations. The capillary pressure – saturation relationship is given in a Van Genuchten formulation. We considered a fracture 10 times smaller (1m) than the one specified in Hydrocoin Level 1 Case 2 geometry (10 m for the left fracture and 15 for the right one).

Fractures dominate the flow, therefore when one parameter of the two (fracture width and fracture permeability) is changed the distribution of the saturations will be more affected. From the saturation fronts we see clearly that in the case with wider fractures the saturation front moves faster which can constitute another proof that the numerical simulator gives trustworthy results.

The differences in the saturation can be compared in Figure 33 where we made a cut at Y=600m. We distinguish two saturation peaks corresponding to the position of the two fractures. In the "original" case (when we have the left fracture width 10 m and the right width 15 m) we see that the between the two peaks saturation is going to 0. In the second case when we assume the 1m fracture width, the influence of the matrix is seen more pregnant, as the DNAPL is forced to infiltrate more in the matrix.

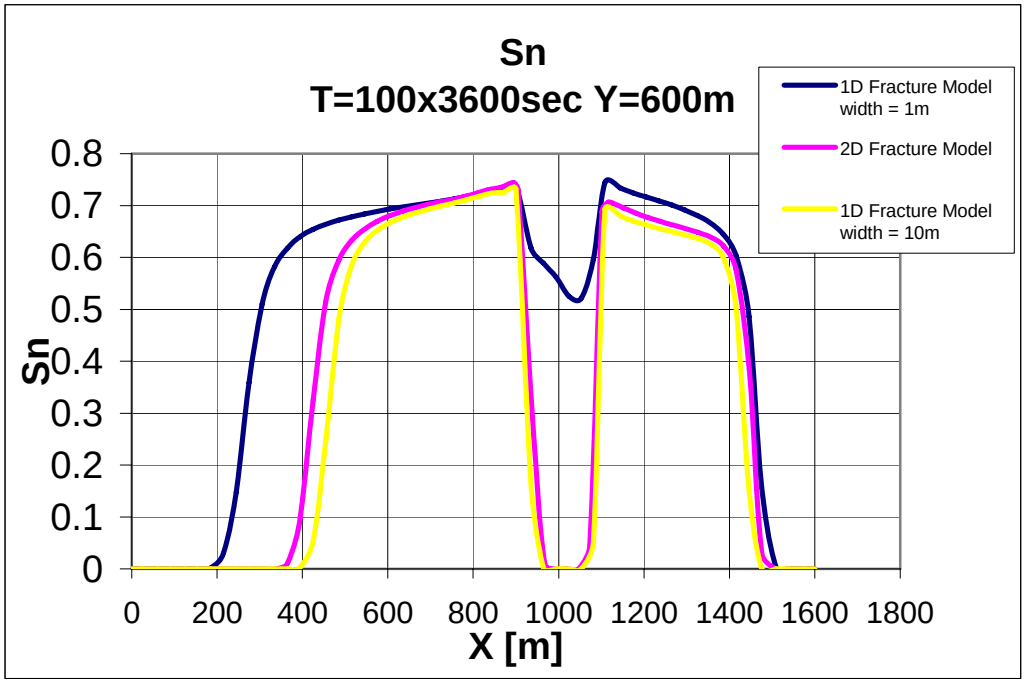

Figure 33: DNAPL saturations at Y=600m and T = 100x3600 for 1D (width 1m and 10m) and 2D fracture model for a Van Genuchten capillary pressure formulation

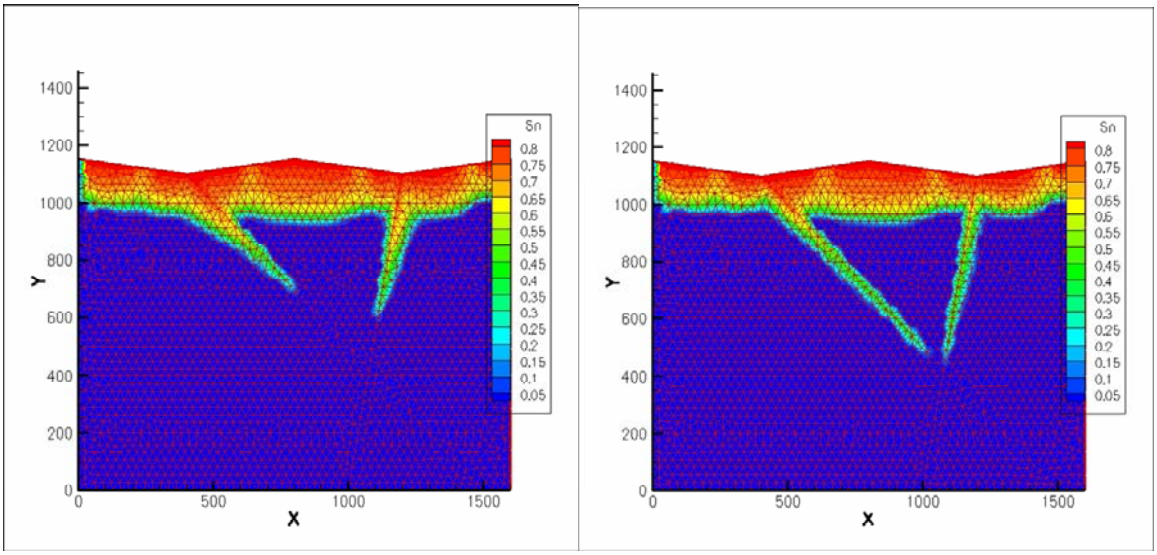

T1 = 20*3600 s **a) width = 1m** **b) width = 10m**

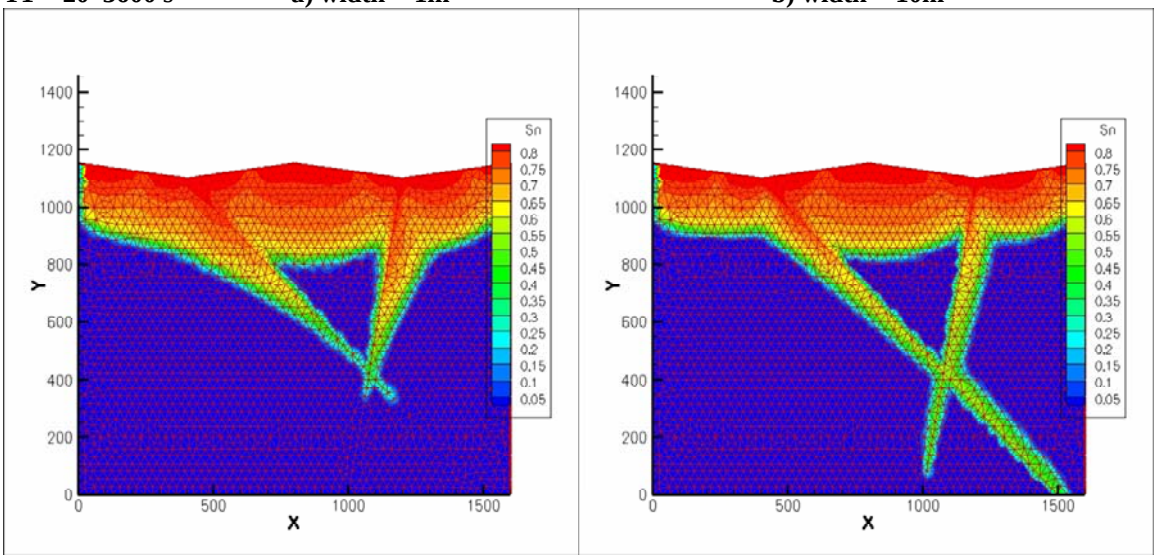

T2 = 40*3600 s **c) width = 1m** **d) width = 10m**

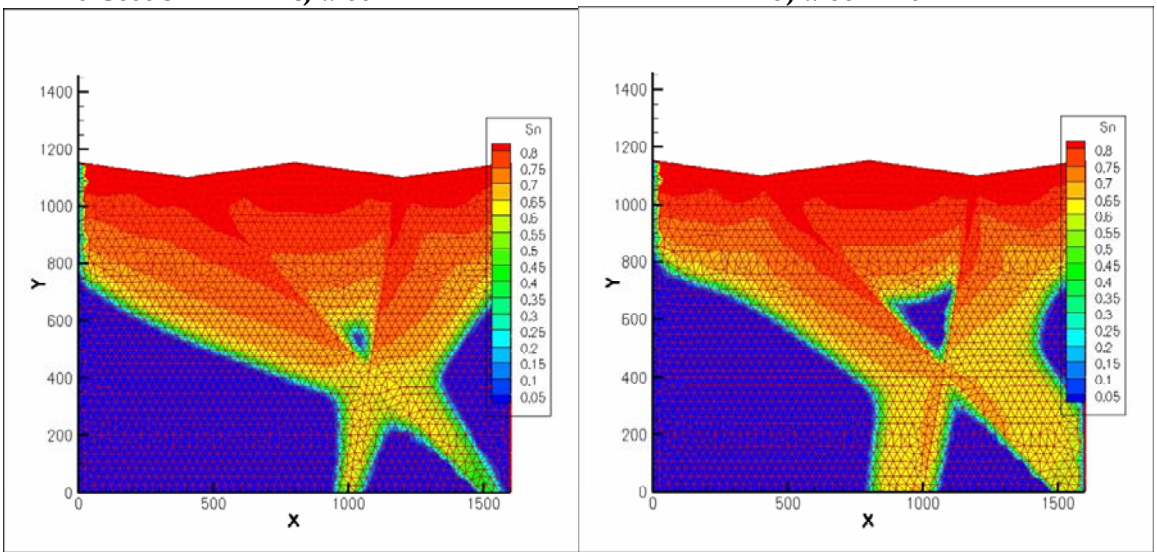

T3 = 100*3600 s **e) width = 1m** **f) width = 10m**

Figure 34: Saturation comparison between different fracture width in 1D fracture models at time T1 = 20x3600 sec, T2 =40 x 3600 sec, T3 =40 x 3600 sec

5.2.1.5 Computation Time

In contrast to the one-phase fracture flow simulation where we obtained similar computation times between the two fracture models, in the two phase fracture flow we have big differences in the computation time. The *1D fracture model* is calculated much faster. For instance the computation time in Brooks-Corey formulation for 1D fracture model is 4.6 times faster than in 2D fracture model.

Table 8: Computation time comparison for 1D and 2D fracture models in two phase flow

Formulation	Km [m^2]	Kf [m^2]	1Df						2Df					
			real		user		sys		real		user		sys	
			min	sec	min	sec	min	sec	min	sec	min	sec	min	sec
BC	1.33E-13	1.33E-10	59	22.962	**54**	53.885	0	5.218	257	17.951	**249**	10.338	0	12.229
VG	1.33E-13	1.33E-10	71	19.643	**68**	11.429	0	6.614	236	46.051	**228**	58.997	0	10.491

A fully coupled, fully implicit, mixed-dimensional vertex centered finite volume method for the discretization of two-phase flow problem on unstructured grids was tested.

A comparison for a 1D fracture model showed that the differences between the lower-dimensional discretization and the equi-dimensional discretization are small. In contrast to the equi-dimensional discretization, the lower-dimensional discretization produces systems which are far easier to solve.

5.2.2 3D geometry

5.2.2.1 Definition of the problem

The third numerical simulator demonstrates the applicability of a lower-dimensional fracture approach in a three dimensional domain for multi-phase flow.

The example shown in Figure 35 was investigated in several research works concerning mesh generation and numerics (*Zielke et al.* [1991], *Barlag et al.* [1998]). *Barlag et al.*[1998] analyzed the heat transport which is characterized by poor advection in the fracture and high diffusion in the matrix.

It consists of a 3D matrix volume with an intersecting 2D fracture. The matrix is subdivided into three blocks with different absolute permeabilities. Km1 = Km2 = 1.32518E-13 m^2 and Km3 = 1.32518E-12. The fracture's absolute permeability is Kf = 1.23907E-07.

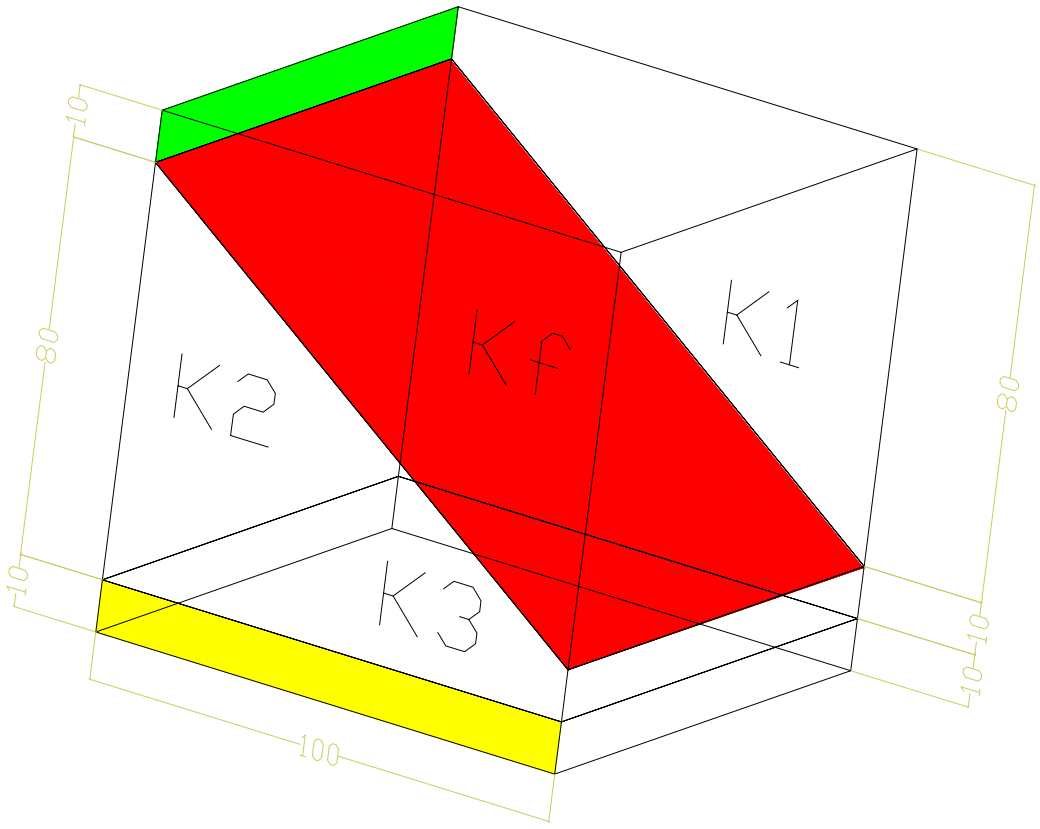

Figure 35: 3D geometry (Zielke et al. [1991])

The boundary conditions for the two-phase fracture flow in the three-dimensional domain are represented in Figure 36.

The geometry is generated in ANSYS ICEM v.11.0 and exported using STAR-CD 3.2.0 solver. The way the geometry is created and the mesh is generated is different than in ART mesh generator.

More characteristics of the generated geometry are specified in Table 9 (i.e. the number and name of the constituent parts and the number of elements for each part). A finer refinement is being created along the fracture.

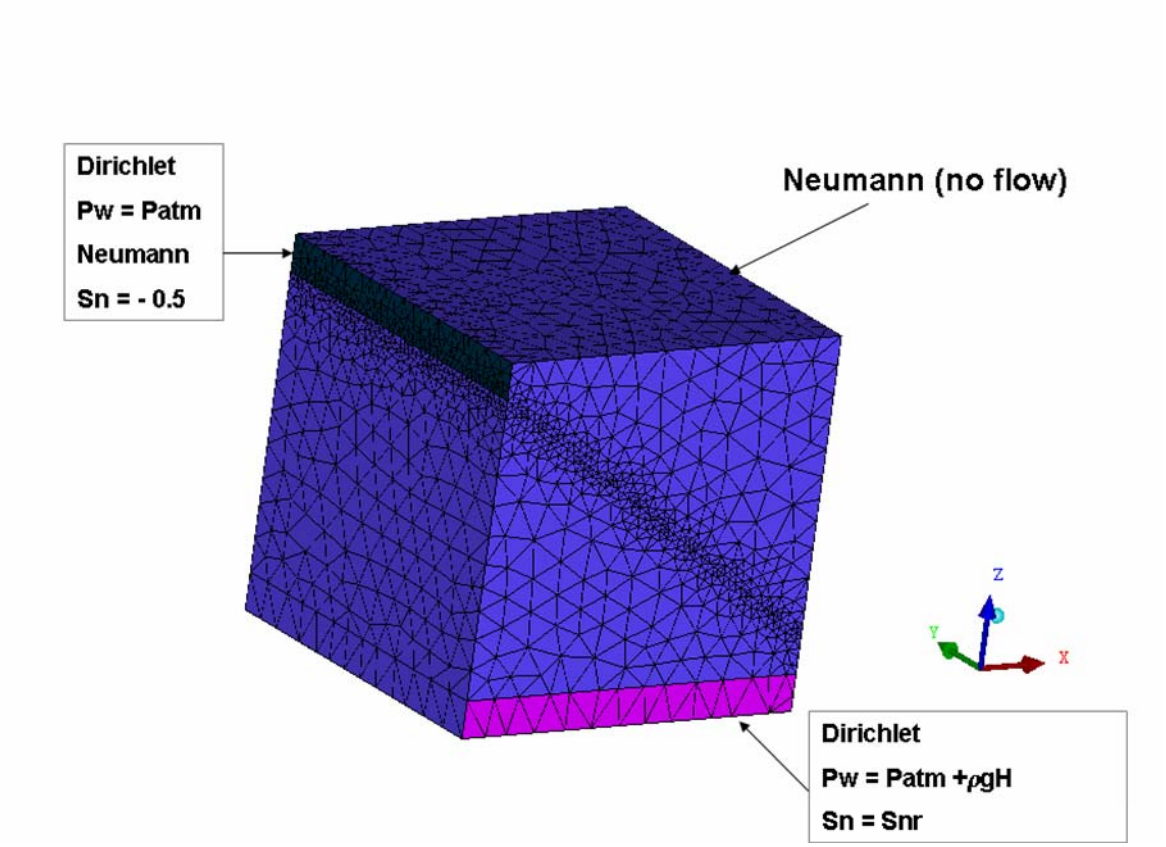

Figure 36: Boundary conditions and the finite element meshes for the 3D domain

Table 9: Geometry information for 3D domain. Number of elements for the different parts of the geometry.

	Part name	Number of elements
1	BODY1 :	74090
2	BODY2 :	73281
3	BODY3 :	2003
4	FRACT :	9357
5	GEOM :	506
6	INFLOW :	252
7	INTERIOR :	346
8	NEUMANN :	3986
9	OUTFLOW :	28
	Total elements :	**163849**
	Total nodes :	**26506**

The input parameters for the two fluid phases are given in Table 10 and Table 11 and the capillary pressure-saturation curves are represented in Figure 37.

Table 10: Input parameters for the two phase fracture-flow problem in 3D domain

	matrix 1, 2	matrix 3	fracture
lambda	2	2	3
pd	500	500	200
Swr	0.1	0.1	0.1
Snr	0.01	0.01	0.01
alpha_VG	0.00158	0.00158	0.0045
n_VG	3.5	3.5	4.3
porosity	0.4	0.5	0.6
Kabs	1.33E-13	1.33E-12	1.24E-07

Table 11: The two fluid properties for the fracture-flow problem in 3D domain

	Water	DNAPL
Density [kg/m^3]	1000	1600
Dyn. Viscosity [kg/m.s]	1.00E-03	5.70E-03

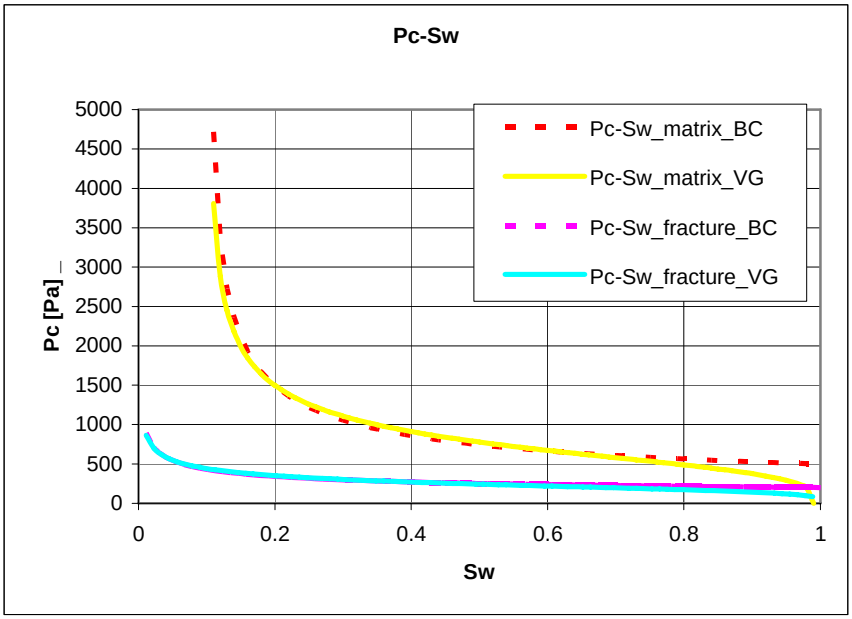

Figure 37: Capillary pressure functions after Brooks Corey and Van Genuchten for 3D domain in the two phase flow problem

The three matrix blocks have the same entry pressure and parameters that determine the capillary pressure-saturation relationships both in Brooks-Corey and in Van Genuchten formulation.

5.2.2.2 Simulation Results

The simulation uses the lower-dimensional centered vertex finite volume method (box fracture method). The time discretization is the implicit backward Euler scheme. The nonlinear equations are solved by inexact Newton linearization which is linearized by Bi-Conjugate Gradient Stabilized solver.

The computation was carried out on parallel computers of 8 nodes. Still the simulation took more than one week. We have used the Brooks-Corey formulation for the capillary pressure saturation relationships for the results plotted in Figure 38.

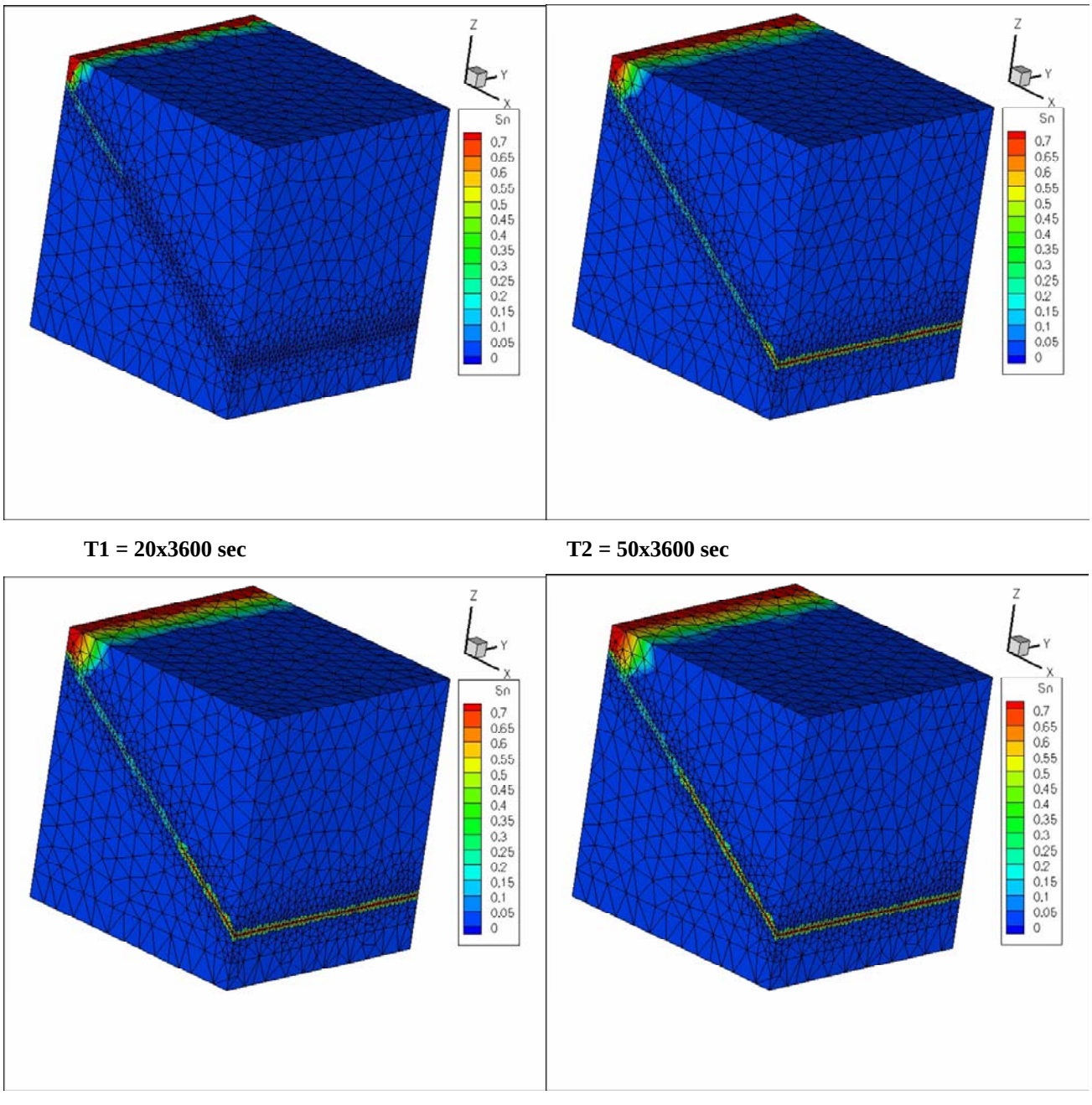

T1 = 20x3600 sec **T2 = 50x3600 sec**

T3 = 70x3600 sec **T4 = 90x3600 sec**

Figure 38: DNAPL front infiltration at different time steps for the 3D domain.

The DNAPL is infiltrating in the upper part and is moving along the fracture. The fracture influence is clearly seen from the beginning of the simulation. Once the saturation front reaches the other end of the 2D fracture another front is starting to move backwards since it cannot surpass the entry pressure of the matrix. This is leading to problems in the convergence of the solution and consequently to high computation times. It is obvious that the capillary forces have in this case a dominating effect.

6 CONCLUSIONS

A small summary of what has been done is given in the following. First there were presented the main fracture models: discrete, multi-continua and hybrid of which it has been shown that the discrete fracture model is numerically superior for the kind of geometries we dealt with in the simulations.

Then there were introduced the mathematical models at the same time with the basic equations for single- and the multi-phase flow in fractured porous media. Due to its advantages the phase-pressure saturation (PPS) formulation was implemented.

After comparing the various finite element methods, the vertex centered finite volume method was picked for solving the fully coupled fully implicit discretization. A special attention was given to the interface conditions that represent the saturation discontinuities in lower- and equi- dimensional elements. It is worth reminding that the vertex-centered finite volume method combines the advantages of the cell centered finite volume discretization and the finite element discretization, and it is not only mass conservative but also can be applied to unstructured grids.

Further on, there have been investigated three different numerical models where fractures are represented as discrete elements. For all experiments was used the unstructured vertex-centered finite volume scheme.

We have tested and demonstrated the capability of MUFTE-UG numerical simulator to solve different ground water problems. For the one phase simulation the results were compared to the ones obtained by other groups in the international hydrologic code intercomparison project HYDROCOIN (1988) and to more recent ones obtained with FEFTRA numerical simulator. The results (i.e. pressure distribution, streamlines) show good agreement between our model and the HYDROCOIN groups. The numerical scheme utilized by FEFTRA for solving the partial differential equations is the conventional Galerkin technique.

One interesting aspect of this research was to compare the results obtained with the lower-dimensional vertex centered finite volume method to the ones having the same dimensional elements in matrix and fracture for one and two fluid phase flow in two and three dimensional domains. The results showed that the differences between the 1D fracture model and the 2D fracture model are small and, accordingly, the capability of MUFTE-UG to implement this model concept both in two and three dimensional domains was demonstrated. Besides this, the lower-dimensional discretization yields systems which are far easier to solve than those from the fully volumetric discretization approach.

In the following, the conclusions after the comparison between the lower- and equi-dimensional fracture models, are grouped into two categories: advantages and disadvantages.

Numerically, the advantages of the lower-dimensional models are summarized as follows:

- the pre-processing is simple and does not require gridding inside the fracture

- avoiding small two or three-dimensional elements (depending on the case) inside the fractures improves the conditioning of the discrete operator and also permits large time steps.

The disadvantages of using lower dimensional elements and approach can be summarized in the following

- Though well-working in a number of applications this lower dimensional approach does not provide local mass conservation and does not allow to follow unambiguous streamlines in and out of the fracture. In some situations this might be a drawback. (Gebauer S. [2002])

- From the numerical simulations was seen that the equidimensional approach ends up with slightly different results.

- A triangulation of the fractures with reasonable number of nodes may lead to long thin elements. Though almost all the degenerate elements are not a problem from the approximation point of view (cf. e.g. *Jamet* [1976]), they cause severe problems in the iterative solution of the discretized problems. For example, classical multigrid methods usually fail for vanishing width of fractures.

In conclusion, it was demonstrated that the lower-dimensional concept is applicable for both 2D and 3D systems and represents correctly the flow in the fractured porous media and the combination of the vertex-centered finite volume method with the discrete fracture model provides a powerful tool to study the multi-phase flow in fractured porous media.

Future work may include the incorporation of more complex mathematical models: multi-phase multi-component simulations or the implementation of different discretizations.

References

1. Atkinson K.E.: “An Introduction to Numerical Analysis”. John Wiley &Sons, Inc. New York. Second Edition, (1988)
2. Aziz, K. and Settari A.: “Petroleum Reservoir Simulation”, Elsevier (1979)
3. Barlag, C.: “Adaptive methods for Modeling Transport Processes in Fractured Subsurface Systems”, 3rd International Conference on Hydroscience and Engineering, (1998)
4. Barenblatt, G.,I. and Zheltov, I.P.: “On fundamental equations of flow of homogeneous liquids in naturally fractured rocks”, Dokl. Akad. Nauk. USSR 132 (3), 545-548, (1960)
5. Bastian P.: “Numerical computation of multi-phase flows in porous media”, Habilitation thesis, Christian-Albrechts-Universitaet Kiel, (1999)
6. Bear, J., Tsang,C.,-H, and De Marsily, G.: 1993 “Flow and Contaminant Transport in Fractured Rock”, Academic Press, San Diego, California, (1993)
7. Bibby, R.: “Mass transport of solutes in dual-porosity media”, Water Resources Res. 17(4), 1075-1081, (1981)
8. Bird, R. B., Stewart, W.E., and Lightfoot E. N.: “Transport Phenomena”, John Wiley, New York, (1960)
9. Bonnet, E., Bour O., Odling N., Main I., Berkowitz B., Davy P., and Cowie P.: “Scaling of fracture systems in geological media”, *Rev. Geophys.*, *39*, 347-383, (2001)
10. Brooks, R.H. and Corey, A.T.,: Hydraulic properties of porous media: Hydrology Papers, Colorado State University, (1964)
11. Brush D. and Thomson N.R. : “Fluid flow in synthetic rough-walled fractures: Navier-Stokes, Stokes, and local cubic law simulations”; Water Resources Research, vol.39, no.4, 1085, (2003)
12. Chavent, G. and Jaffré J. : “Mathematical Models and Finite Elements for Reservoir Simulation”, North-Holland, (1978)
13. Duijn C.J. van, Molenaar J., De Neef M.J. : “The effect of capillary forces on immiscibe two-phase flow in heterogeneous porous media”; Trans. Porous Media 21, 71-93, (1995)
14. Ersland B.G. et al.: “Numerical methods for flow in a porous medium with internal boundaries” Computational Geosciences 2, p217-240, (1998)
15. Fuchs, A.: “Optimierte Delauney-Triangulation zur Vernetzung getrimmter NURBs-Körper, Dissertation”, Shker Verlag, (1999)
16. Gebauer S., Neunhäuserer L. , Kornhuber R., Ochs S., Hinkelmann R., Helmig R.: “Equidimensional modeling of flow and transport processes in fractured porous systems” , International Conference on Computational Methods in Water Resources, Delft, (2002)
17. Geiger S., Niessner J., Matthäi S., Helmig R.: “Black-Oil Simulations for Three-Component Three-Phase Flow in Fractured Porous Media”; SPE International, (2007)
18. Genuchten, M.Th. van,: “ A closed-form equation for predicting the hydraulic conductivity of unsaturated soils”. Soil.Sci.Soc.Am. J44:892-898, (1980)
19. Helmig R.: “Multiphase flow and transport processes in the subsurface – a contribution to the modeling of Hydrosystems”, Berlin: Springer-Verlag, (1997)
20. Hinkelmann R.: “Efficient numerical methods and information-processing techniques in environment water”. Institut für Wasserbau – Universität Stuttgart, (2003)
21. Hornung, U., editor: “Homogenization and Porous Media, volume 6 of Interdisciplinary Applied Mathematics”. Springer-Verlag, Berlin, Heidelberg, New York, (1997)
22. Hoteit H., Firoozabadi A., “Multicomponent fluid flow by discontinuous Galerkin and mixed methods in unfractured and fractured media”
23. Huyakorn, P.,S., Lester, B.H. and Mercer, J.,W.: “An efficient finite element technique for modeling transport in fractured porous media, 1, single species transport”, Water Resources Res. 19(3), 841-854, (1983)

24. Jamet P.: “Estimation d’erreur pour des elements finis droits Presque degeneres”; R.A.I.R.O., Serie Analyse Numerique, 10, No.3, p.43-61, (1976)
25. Juanes R., Samper J., Molinero J.: “A general and efficient formulation of fractures and boundary conditions in the finite element method”, International Journal for Numerical Methods in Engineering; 54:1751-1774, (2002)
26. Karimi-Fard M., Durlofsky L.J., Aziz K.: “An Efficient Discrete-Fracture Model Applicable for General-Purpose Reservoir Simulators” SPE J. , 9, 227-236, (2004)
27. Karimi-Fard M., Firoozabadi A.: “Numerical Simulation of Water Injection in 2D Fractured Media Using Discrete-Fracture Model” (2001)
28. Löfman, Jari, Keto, Vesa & Mészáros, Ferenc : “FEFTRATM. Verification. Espoo 2007. VTT” Tiedotteita Research Notes 2385. 103 p. + app. 4 p, (2007)
29. Molenar J.: “Multigrid methods for fully implicit oil reservoir simulation”, In Proceedings Copper Mountain Conference on Multigrid Methods (1995)
30. Niessner et al.: “Interface condition and linearization schemes in the Newton iterations for two-phase flow in heterogeneous porous media”, Advances in Water Resources 28, 671-687, (2005)
31. Oian E. , Berg S. S.: “Hierarchical approach for simulating fluid flow in normal fault zones”, Petroleum Geoscience, Vol.13, No.1, pp.25-35, (2007)
32. Peaceman, D.W. : “Fundamentals of Numerical Reservoir Simulation”, Elsevier, (1977)
33. Reichenberger V., Jakobs H., Bastian P., Helmig R., Niessner J., “Complex Gas-Water Processes in Discrete Fracture-Matrix Systems: Up-scaling, Mass-Conservative Discretization and Efficient Multilevel Solution”; Institut für Wasserbau, Universität Stuttgart, Heft 130, (2004)
34. Reichenberger V., Jakobs H., Bastian P., Helmig R.,: A mixed-dimensional finite volume method for two-phase flow in fractured porous media; Advances in Water Resources 29, 1020-1036, (2006)
35. Royer P. ,Auriault J.-L., Lewandowska J., Serres C. “Continuum Modeling of Contaminant Transport in Fractured Porous Media”; Kluwer Academic Plubishers (2002)
36. Sahimi, M., “Flow and Transport in Porous Media and Fractured Rock: From Classical Methods to Modern Approaches”, VCH, Weinheim, (1995)
37. Singhal B.B.S. and Gupta R. P. : “Applied Hydrogeology of Fractured Rocks”. Kluwer Academic Publishers, Dordrecht, Boston, London, (1999b)
38. Wu Y.-S. and Pruess, K., “Numerical simulation of non-isothermal multiphase tracer transport in heterogeneous fractured porous media”. Advances in Water Resources, 23:699-723, (2000)
39. Zielke, W., Helmig, R., Kröhn, K.-P., Shao,H., Wollrath, J.: “Discret Modelling of Transport Processes in Fractured Porous Rock” in Wittke (editor): International Congress on Rock Mechanics, 57-60, International Society for Rock Mechanics, (1991)

APPENDIX

Structure of the Application Example for one phase flow in 1D fracture model (SIM_1D_frac)

The development in MUFTE of numerical simulation of one-phase flow for the HYDROCOIN (1998) geometry assuming fractures as one dimensional elements is presented here. The application name is k1 and the folder name containing the application has been given "SIM_1D_frac". This chapter contains the overview of all files of the application problem k1.

The application directory SIM_1D_frac contains the following files:

- C-file: *initall.c*
- C-file: *k1_fflow.c*
- C-file: *k1_ftransp.c*
- C-file: *q_fbvp.c*
- Script-file: *k1_ftitrp.scr*
- defaults
- Makefile

- **Script file *k1_ftitrp.scr***

The interaction between MUFTE application and the UG-library is being done by the scrip-file. All the commands used in the script file are defined in ug/ui/commands.c. The fracture-matrix domain is previously discretized using ART and the files *q.bnd* and *q.net* provide the domain and the mesh information.

The script-file opens with the *logon* command which controls the output to a log-file. In the same way the file ends with a *logoff* command.

```
#########################################################
#open log file
#########################################################
logon k1_ftitrp.log;
```

Afterwards are defined the main parameters of the simulation.

```
#########################################################
# some constants
#########################################################
BASELEVEL       = 0;          # start from this level
MAXLEVEL        = 0;          # finest level
DOGLS           = 0;          # plot matrix;
DOGRAPHICS      = 1;          # plot results

DOFILMS         = 1;            # do output either tecplot or dataxplorer film
DOTECPLOT       = 1;            # do tecplot film
DODX            = 0;
TECPLOTINC      = 10;           # no of time-steps per frame

fsteps          = 350;          # total number of time steps for flow (>1!)
tsteps          = 10;           # total number of time steps for transport
DTSTART         = 10;           # initial time step
```

```
DT              = 10;           #
END             = 100*86400.0;  # end of simulation time
DTMIN           = 1;            # smallest time step

#########################################################
# create coarse mesh
#########################################################

readartbnd q.bnd;
new fractk1 $b qBVP $f FlowTIFormat $h @HEAP;
readartnet q.net;

refreshon;
fixcoarsegrid;
@gw;
```

The flow and transport variables in the single-phase problem as well as the values of the boundary conditions are defined in the script-file.

```
#########################################################
# initialize input data
#########################################################
# BVP values
source = 6.0E-08;  # [kg/sm^2]
time1 = 30;

thickness = 1.0;      # Set to 1.0 for 3D applications
fract1_width = 10.0;
fract2_width = 15.0;
fract1_prop = -1.0;
fract2_prop = -2.0;

k_x_1 = 1.32518E-15;         # [m^2] matrix permeability
k_y_1 = 1.32518E-15;         # [m^2]
k_z_1 = 1.32518E-15;         # [m^2]

fract1_k_0 = 1.32518E-12;       # [m^2] fracture 1 permeability
fract2_k_0 = 1.32518E-13;       # [m^2] fracture 2 permeability

flow_visc = 0.0013;      # dynamic viscosity!!! (water)
flow_dens = 1000.0;      # water
dens_mode = 0;           # 0=incompressible, 1=compressible
                         # For dens_mode = 1: If not air, change
stor_coeff = 1.0e-4;         # only needed for dens_mode = 1
fract_stor_coeff = 1.0e-4;   # only needed for dens_mode = 1

mat_poros = 0.13;         # used for transport and dens_mode = 1
fract1_poros = 0.30;      # used for transport and dens_mode = 1
fract2_poros = 0.30;      # used for transport and dens_mode = 1

# transport values
tracer_dens = 1.0;        # If 1 - same as fluid. Output conc [kg(subst.)/m^3(mixture)]
mat_disp_l = 1.0e-9;      # alpha_l (minimized)
mat_disp_t = 1.0e-9;      # alpha_t (minimized)
fract1_disp_l = 0.0;
fract2_disp_l = 0.0;
mol_diff_fract = 1.0e-9;  # Deff (minimized)
mol_diff_mat   = 1.0e-9;  # Deff (minimized)
```

The values for several parameters describing the fluid porous-medium properties or the interaction between fluid and matrix are set in the following. The functions will be later described in the c-files.

For steady state:

```
#########################################################
# set up steady state discretization scheme
#########################################################
npcreate fk1f $c fk1f;
npinit fk1f $p pressure;

npcreate fbf $c fbf;
npinit fbf $A MAT $x pressure $b rhs $P fk1f;


#########################################################
# set up steady state flow solver
#########################################################
npcreate ilu $c ilu;
npinit ilu $damp 1.0;

npcreate base $c ex;
npinit base;

npcreate basesolver $c ls;
npinit basesolver $red 1.0E-4 $m 50 $I base $display no;

npcreate transfer $c transfer;
npinit transfer $x pressure $S 2.0;

npcreate lmgc $c lmgc;
npinit lmgc $S ilu ilu basesolver $T transfer $n1 2 $n2 2 $g 1;

npcreate mgs $c bcgs;
npinit mgs $A MAT $x pressure $b rhs $m 25 $red 1.0E-6
           $abslimit 1.0E-15 $I lmgc $display full;
```

For transient flow:

```
#########################################################
# set up transient flow discretization scheme
#########################################################
npcreate fbfti $c fbfti;
npinit fbfti $FP fk1f;

#########################################################
# set up transient flow solver
#########################################################

#grid transfer numproc
npcreate fti_transfer $c transfer;
npinit fti_transfer $x pressure $S 2.0;

#linear solver and iteration numprocs
npcreate fti_smooth $c sgs;
npinit fti_smooth $damp 1.0;

npcreate fti_base $c ex;
npinit fti_base;
```

```
npcreate fti_basesolver $c ls;
npinit fti_basesolver $abslimit 1.0E-15 $red 0.001 $m 10 $I fti_base;

npcreate fti_lmgc $c lmgc;
npinit fti_lmgc $S fti_smooth fti_smooth fti_basesolver $T fti_transfer
               $n1 2 $n2 2 $g 1 $b 0;

npcreate fti_mgs $c bcgs;
npinit fti_mgs $abslimit 1.0E-15 $m 40 $I fti_lmgc $display full;

# nonlinear solver numproc to be used by time solver
npcreate fti_newton $c newton;
npinit fti_newton $abslimit 1.0E-8 $red 1.0E-10 $T fti_transfer $S fti_mgs
             $rhoreass 0.8 $lsteps 6 $maxit 50 $line 1 $linrate 0
             $lambda 1.0 $linminred 1.0E-5 $divfac 1.0E100 $display red;

# the time solver
npcreate fti_ts $c bdf;
npinit fti_ts $y pressure $A fbfti $S fti_newton $T fti_transfer
            $baselevel 0 $order 1 $predictorder 0 $nested 0
            $dtstart @DT $dtmin @DTMIN $dtmax @DT $dtscale 1.0 $rhogood 0.001;

##########################################################
# set up transport discretization scheme
##########################################################
npcreate fk1t $c fk1t;
npinit fk1t;

npcreate fbt $c fbt;
npinit fbt $FP fk1f $TP fk1t $alpha 1.0 $so 0 $calc 0;

##########################################################
# set up transport solver
##########################################################

#grid transfer numproc
npcreate t_transfer $c transfer;
npinit t_transfer $x sol $S 2.0;

#linear solver and iteration numprocs
npcreate t_smooth $c sgs;
npinit t_smooth $damp 1.0;

npcreate t_base $c ex;
npinit t_base;

npcreate t_basesolver $c ls;
npinit t_basesolver $abslimit 1.0E-15 $red 0.001 $m 10 $I t_base;

npcreate t_lmgc $c lmgc;
npinit t_lmgc $S t_smooth t_smooth t_basesolver $T t_transfer $n1 2 $n2 2
             $g 1 $b 0;

npcreate t_mgs $c bcgs;
npinit t_mgs $abslimit 1.0E-15 $m 40 $I t_lmgc $display full;

# nonlinear solver numproc to be used by time solver
npcreate newton $c newton;
```

```
npinit newton $abslimit 1.0E-15 $red 1.0E-5 $T t_transfer $S t_mgs
              $rhoreass 0.8 $lsteps 6 $maxit 50 $line 1 $linrate 0
              $lambda 1.0 $linminred 1.0E-5 $divfac 1.0E100 $display red;

# the time solver
npcreate t_ts $c bdf;
npinit t_ts $y Concentration $A fbt $S newton $T t_transfer
            $baselevel 0 $order 1 $predictorder 0 $nested 0
            $dtstart @DT $dtmin @DTMIN $dtmax @DT $dtscale 1.0 $rhogood 0.001;
```

The discretization scheme, the multigrid cycles, the time solver have to be initialized with their parameters. Also the sequence of the simulation process is defined. This includes initializing the time step, defining the first time step and defining the processes of the time loop.

```
##########################################################
# initialize time step
##########################################################
npexecute fti_ts $pre $init;
@plotw;
@tplflow;

##########################################################
# do FIRST time step
##########################################################
fstep=1;
print "[[[ TIMESTEP ", fstep;
resetclock;
getbndfluxti = 2;
npexecute fti_ts $bdf1;
readclock;
print "]]] TIMESTEP: ", fstep, " TIME: ", TIME, " DT: ", TIMESTEP, " RUNTIME: ", CLOCK;
@plotw;
@tplflow;
if (fstep==fsteps) break;

##########################################################
# time loop
##########################################################
repeat {
    fstep=fstep+1;
    print "[[[ TIMESTEP ", fstep;
    resetclock;
    getbndfluxti = 2;
    npexecute fti_ts $bdf1;
    readclock;
    print "]]] TIMESTEP: ", fstep, " TIME: ", TIME, " DT: ", TIMESTEP, " RUNTIME: ", CLOCK;
    @plotw;
    @tplflow;
    if (fstep==fsteps) break;
    if (TIME > END) break;
}
```

- **Boundary condition file *q_fbvp.c:***

At the beginning the function to initialize the domain with the given boundary conditions is being defined. Thus, the values of the boundary conditions defined in the script-file are read and stored.

```
/*************************************************************************/
/* read in constant boundary conditions and more*/
/*************************************************************************/

        static DOUBLE
        source,time1,fract1_width,fract1_prop,fract2_width,fract2_prop;

        static INT FractK1ProblemConfig (INT argc, char **argv)
        {
              /* read a string variable */
              GetStringValueDouble("upper_p",&upper_p);
              GetStringValueDouble("lower_p",&lower_p);
              GetStringValueDouble("source",&source);
              GetStringValueDouble("time1",&time1);
              GetStringValueDouble("fract1_width",&fract1_width);
              GetStringValueDouble("fract1_prop",&fract1_prop);
              GetStringValueDouble("fract2_width",&fract2_width);
              GetStringValueDouble("fract2_prop",&fract2_prop);
              return(0);
        }
```

The boundary conditions are defined in the following. For the North Boundary the head is defined as

$$h(x,y) = y$$

so two functions have to be defined, respectively for the descending and ascending slope. The two functions are called K1ProblemInBoundary1 and K1ProblemInBoundary2.

```
        static INT K1ProblemInBoundary1 (void *segdata, void *conddata, DOUBLE *in, DOUBLE *outValues, INT
        *bndType)
        {

            DOUBLE time;
            DOUBLE lambda;

            lambda = in[0];
            time = in[IN_T];

            bndType[OUT_BNDTYP_fit] = DIRICHLET;
            bndType[OUT_BNDTYP_fti] = DIRICHLET;

            outValues[OUT_BNDVAL_fit]      = 9.81*1000*(150-lambda*50);
            outValues[OUT_BNDVAL_fti]      = 9.81*1000*(150-lambda*50);

            bndType[OUT_BNDTYP_trp] = NEUMANN;
            outValues[OUT_BNDVAL_trp]      = source;

            if (time <= time1) {
               outValues[OUT_BNDVAL_trp] = source;
            }
            else {
               outValues[OUT_BNDVAL_trp] = 0.0;
            }

                return(0);
        }
        static INT K1ProblemInBoundary2 (void *segdata, void *conddata, DOUBLE *in, DOUBLE *outValues, INT
        *bndType)
        {
```

```
    DOUBLE time;
    DOUBLE lambda;

    lambda = in[0];
    time = in[IN_T];

    bndType[OUT_BNDTYP_fit] = DIRICHLET;
    bndType[OUT_BNDTYP_fti] = DIRICHLET;

    outValues[OUT_BNDVAL_fit]      = 9.81*1000*(lambda*50+100);
    outValues[OUT_BNDVAL_fti]      = 9.81*1000*(lambda*50+100);

    bndType[OUT_BNDTYP_trp] = NEUMANN;
    outValues[OUT_BNDVAL_trp]      = source;

    if (time <= time1) {
       outValues[OUT_BNDVAL_trp] = source;
    }
    else {
       outValues[OUT_BNDVAL_trp] = 0.0;
    }

        return(0);
}
```